

**Parameter Optimization of Optical Materials
and Investigation of
Surface Plasmon Polariton (SPP) Propagation in
Plasmonic Waveguide**

by

Mehedi Islam (102471)

Md. Nazmul Islam (102413)

Monzurul Islam (102467)

A Thesis Presented

in Partial Fulfillment of the Requirements for the Degree of

BACHELOR OF SCIENCE

IN

ELECTRICAL AND ELECTRONIC ENGINEERING

ISLAMIC UNIVERSITY OF TECHNOLOGY (IUT)

A Subsidiary Organ of Organization of Islamic Cooperation (OIC)

Dhaka, Bangladesh.

November, 2014

©2014 Mehedi Islam, Md. Nazmul Islam and Monzurul Islam

All Rights Reserved.

Declaration of Authorship

We, Mehedi Islam (102413), Md. Nazmul Islam (102413) and Monzurul Islam (102467), declare that this thesis titled, 'Parameter Extraction of Optical Materials and Investigation of Surface Plasmon Polariton (SPP) Propagation in Plasmonic Waveguide' and the works presented in it are our own. We confirm that:

- This work has been done for the partial fulfillment of the Bachelor of Science in Electrical and Electronic Engineering degree at this university.
- Any part of this thesis has not been submitted anywhere else for obtaining any degree.
- Where we have consulted the published work of others, we have always clearly attributed the sources.

Submitted By:

Mehedi Islam (102471)

Md. Nazmul Islam (102413)

Monzurul Islam (102467)

Parameter Optimization of Optical Materials and Investigation of Surface Plasmon Polariton (SPP) Propagation in Plasmonic Waveguide

Approved by

Md. Ghulam Saber

Thesis co-supervisor,
Lecturer,
Department of Electrical and Electronic Engineering,
Islamic University of Technology.

Rakibul Hasan Sagor

Thesis Supervisor,
Assistant Professor,
Department of Electrical and Electronic Engineering,
Islamic University of Technology.

Prof. Dr. Md. Shahid Ullah

Head of the Department,
Department of Electrical and Electronic Engineering,
Islamic University of Technology.

Abstract

When free electrons inside the metal get affected, they start to oscillate. The movement of this oscillation inside the metal is called plasmon. The excitation can be done by exposing metal to a photon. Surface Plasmon-Polariton is formed when coupling between a plasmon inside the metal and photon outside the metal happens, and they travel at the same speed. SPPs can be used as an alternative medium for transmitting signals as it can overcome the light diffraction limit. But the main limitation of SPP is higher propagation loss in metal and short propagation distance not exceeding micrometers. The main goal of this thesis is to optimize the modeling parameters for several optically valued materials and analyze their performance in FDTD. Lorentz model and modified Lorentz model parameter of several optically valued material has been optimized using large scale nonlinear algorithm. SPP propagation characteristics through dielectric-metal-dielectric waveguide have been investigated to analyze the performance of one of the optimized dielectric material.

Acknowledgements

First and foremost, we offer gratitude to the Almighty Allah (SWT) for giving us the capability to do this work with good health. We are grateful to our research supervisor, Rakibul Hasan Sagor and co-supervisor Md. Ghulam Saber for the support and guidance throughout our research at Islamic University of Technology (IUT) since July, 2013. He created a research environment for which we were able to explore many ideas without constraint. We have gained a wealth of knowledge and experience in science and engineering through his direction that is beyond value to our future endeavor. For these things, we give many thanks to him. We would like to thank all the faculty members of the department of EEE, IUT for their inspiration and help. And last but not the least we are thankful to our family, friends and well-wishers for their support and inspiration. Without them it would never have been possible for us to make it this far.

TABLE OF CONTENTS

List of Figures	9
List of Tables	10
ABBREVIATIONS	11
Chapter 1	13
Introduction and Background	13
1.1 Introduction.....	13
1.2 Literature Review.....	14
1.3 Thesis Objective.....	15
1.4 Thesis Organization	16
Chapter 2.....	17
SPP Propagation Theory	17
2.1 Introduction.....	17
2.2 SPP at Single Interface.....	20
2.3 SPP at Double Interface	23
Chapter 3.....	24
Material Modeling Within Optical Range	24
3.1 Introduction.....	24
3.2 Different Material Models	26
3.2.1 The Debye Model	26
3.2.2 The Lorentz Model	28
3.3 Material Dispersion.....	31
Chapter 4.....	33
Overview of Finite-Difference Time Domain Method	33
4.1 The Yee Algorithm	33
4.1.1 One-Dimensional Simulation.....	37
4.1.2 Two-Dimensional Simulation.....	38
4.2 Stability	41
4.3 Absorbing Boundary Condition	42

4.4	Material Dispersion in the FDTD	47
4.4.1	The Auxiliary Differential Equation (ADE)	47
4.4.2	Z-Transformation	49
4.4.3	Recursive Convolution.....	50
Chapter 5	51
	Parameter Optimization of Optical Materials	51
5.1	Material Models	51
5.1.1	Lorentz Model.....	51
5.1.2	Modified Lorentz Model.....	52
5.2	Optimized Materials.....	53
5.3	Optimization Method	54
5.4	Optimized parameters	56
5.4.1	Optimized parameter for Dielectric material for Lorentz model	56
5.4.2	Optimized parameter for Dielectric material for modified Lorentz model	58
5.4.3	Optimized parameter for Metal for modified Lorentz model	60
Chapter 6	67
	Application and Case Study	67
6.1	Simulation model	67
6.2	Numerical Results for Temporal Solitons.....	68
6.3	Plasmonic Waveguide.....	69
Chapter 7	77
	Conclusion and Future Works	77
7.1	Summary and Conclusion	77
7.2	Future Works	78
Bibliography	79

List of Figures

FIGURE 2.1: BASIC CONFIGURATION OF A PLASMONIC CHIP THAT USE DIFFRACTIVE OPTICS TO EXCITE THE SPP AND TO OUTCOUPLE THE EMITTED LIGHT.....	20
FIGURE 2.2: SPP AT THE SINGLE INTERFACE	22
FIGURE 2.3: SPP AT THE DOUBLE INTERFACE.....	23
FIGURE 3.1: FORCES ACTING IN LORENTZ MODEL.....	29
FIGURE 4.1: ESTIMATION FOR THE DERIVATIVE OF $f(x)$ USING FORWARD, BACKWARD AND CENTRAL-DIFFERENCE	35
FIGURE 4.2: YEE'S SPATIAL GRID SHOWING ELECTRICAL AND MAGNETIC FIELD COMPONENT PER CELL..	36
FIGURE 4.3: UPDATING FIELD VALUES USING LEAP FROG METHOD	41
FIGURE 4.4: PML SETUP.....	44
FIGURE 4.5: PROPOGATION OF ELECTRIC FIELD AT TIME STEP, $T=5$	45
FIGURE 4.6: PROPOGATION OF ELECTRIC FIELD AT TIME STEP, $T=18$	45
FIGURE 4.7: PROPOGATION OF ELECTRIC FIELD AT TIME STEP, $T=38$	46
FIGURE 4.8: PROPOGATION OF ELECTRIC FIELD AT TIME STEP, $T=70$	46
FIGURE 5.1: CURVE FITTING FOR CRYSTALLINE ARSENIC SULFIDE.....	57
FIGURE 5.2: CURVE FITTING FOR YTTRIUM ALUMINUM GARNET	57
FIGURE 5.3: CURVE FITTING FOR SILICON CARBIDE.....	57
FIGURE 5.4: CURVE FITTING FOR SILICON MONOXIDE	59
FIGURE 5.6: CURVE FITTING FOR NICKEL	63
FIGURE 5.5: CURVE FITTING FOR IRIDIUM	63
FIGURE 5.7: CURVE FITTING FOR HEXAGONAL COBALT	64
FIGURE 5.9: CURVE FITTING FOR TITANIUM	65
FIGURE 5.10: CURVE FITTING FOR COPPER.....	65
FIGURE 5.11: CURVE FITTING FOR PLATINUM	65
FIGURE 6.1 CALCULATED OPTICAL PULSE AFTER 20,000 AND 40,000 TIME-STEPS	69
FIGURE 6.2: SCHEMATIC DIAGRAM OF THE DMD WAVEGUIDE USED FOR SIMULATION.	70
FIGURE 6.3: E_x PROFILE PUMPED INTO DMD WAVEGUIDE	71
FIGURE 6.4: H_y PROFILE PUMPED INTO DMD WAVEGUIDE.....	71
FIGURE 6.5: E_x PROFILE AT DIFFERENT TIME INSTANT.....	72
FIGURE 6.6: E_z PROFILE AT DIFFERENT TIME INSTANT.....	72
FIGURE 6.7: H_y PROFILE AT DIFFERENT TIME INSTANT	73
FIGURE 6.8: E_x FIELD STRENGTH AT DIFFERENT DISTANCE	73
FIGURE 6.9: E_z FIELD STRENGTH AT DIFFERENT DISTANCE	74
FIGURE 6.10: H_y FIELD STRENGTH AT DIFFERENT DISTANCE.....	74
FIGURE 6.11: 2D ELECTRIC FIELD DISTRIBUTION INSIDE THE DMD WAVEGUIDE USED FOR SIMULATION AT TIME STEP (A) 100 (B) 500 (C) 950 (D) 1400 (E) 1750 (F) 2646.....	75
FIGURE 6.12: POWER TRANSMISSION EFFICIENCY AT DIFFERENT DISTANCES.....	76

List of Tables

TABLE 5.1: OPTIMIZED PARAMETER FOR CRYSTALLINE ARSENIC SULFIDE, YTTRIUM ALUMINUM GARNET, SILICON CARBIDE FOR LORENTZ MODEL.....	56
TABLE 5.2: OPTIMIZED PARAMETER FOR SILICON MONOXIDE FOR MODIFIED LORENTZ MODEL .	58
TABLE 5.3: OPTIMIZED PARAMETER FOR SEVEN METALS FOR MODIFIED LORENTZ MODEL	60
TABLE 5.3: OPTIMIZED PARAMETER FOR SEVEN METALS FOR MODIFIED LORENTZ MODEL (CONTINUED).....	61

ABBREVIATIONS

FDTD	Finite Difference Time Domain
ADE	Auxiliary Difference Equation
ABC	Absorbing Boundary Condition
PML	Perfectly Matched Layer
TM	Transverse Electric
TE	Transverse Magnetic
SPP	Surface Plasmon Polariton
MDM	Metal-Dielectric-Metal
DMD	Dielectric-Metal-Dielectric
PLRC	Piecewise Linear Recursive Convolution
MLM	Modified Lorentz Model

Dedicated to our parents.....

Chapter 1

Introduction and Background

1.1 Introduction

The photon is an electromagnetic wave that can be considered as the unit of light. Circuits and devices controlling electrons are called “electronics”. In the same analogy, circuits and devices controlling photons are called “photonics”.

Plasmonics forms a major part of the fascinating field of nanophotonics, which explores how electromagnetic fields can be confined over dimensions on the order of or smaller than the wavelength. It is based on interaction processes between electromagnetic radiation and conduction electrons at metallic interfaces or in small metallic nanostructures, leading to an enhanced optical near field of sub-wavelength dimension. At present, the communication system is fully dependent on the optical fibers which offer high bandwidth and low loss than electronic interconnections. The same advantage can be availed if the optical technology is used in computer chips. Also, the optical chips will not require any insulation since photons do not interact with each other, making the system lighter. According to the diffraction limit rule, light cannot propagate through aperture that is smaller than half of its wavelength. But this diffraction limit can be overcome by using a new type of electromagnetic wave called Surface-Plasmon-Polariton (SPP) that is generated at the metal surface due to the coupling of photon and electron when metal is exposed to light in a certain way. SPPs in certain conditions propagate on the surface of the metal no matter what is the dimension. This property of SPP will enclose a new horizon in technological advancement. If plasmon based integrated circuits are used, there will be a dramatic

increase in computation power chips and hopefully in the near future plasmon based chips will be available. Researchers have achieved enormous performance improvement in solar cell technology using plasmonics. The absorption efficiency has increased significantly by implementing plasmon enhanced solar cells [1-3]. Plasmonics is also being applied in the field of imaging [4-7] biosensing [8], bragg reflector [9] and metamaterials [10].

1.2 Literature Review

We shall discuss prospects for using numerical solutions of Maxwell's equations, in particular Finite-Difference-Time-Domain (FDTD) method to innovate and design key electrical engineering technologies ranging from cellphones and computers to lasers and photonic circuits. Overall, FDTD technique is marching-in-time procedure that simulates the continuous actual electromagnetic waves in a finite spatial region by sampled-data numerical analogous propagating in a computer data space[11]. In this section our focus will be on published works done on different types of material modelling using Finite-Difference-Time-Domain (FDTD) based various models (Like as: Drude Model, Debye Model, Lorentz Model, Lorentz Drude Model, Modified Lorentz Model) and extract the optical parameters.

T. Onuki et al.[12] studied the propagation of plasmons on gold nanowires [13] experimentally. The experiments were done on two different nanowires, one 2 μm long and the other 6 μm long. The results were compared to numerical simulations from FDTD, and they showed agreement on propagation length. Hochberg et al [14] showed that light can also be efficiently coupled between more conventional silicon waveguides and these plasmonic waveguides with compact couplers. Metal was modeled also by the Debye model [15].

Krug et al. [16] have reported the gold parameters that are applicable in the wavelength range of 700-1000 nm. Pernice et al.[17] have extracted the parameters for Nickel using Lorentz-Drude model. A.D. Rakic et al.[18] have reported the parameters for Nickel, Palladium, Titanium and 8 other metals using Lorentz-Drude and Brendel-Bormann Model.

1.3 Thesis Objective

The main objective of the thesis is to extract the modeling parameters for different linear dispersive material and use those material modeling parameters to study the SPP propagation in different optical nanostructures. However, more specifically, the objectives are

- To extract the modeling parameters for different metals and dielectric materials.
- To develop a simulation based model on the FDTD method that is capable of simulating the properties of linear dispersive materials.
- Using the FDTD simulator to study plasmonic waveguides.
- To investigate the symmetric SPP propagation properties in dielectric-metal-dielectric waveguide.
- To summarize important conclusions from the obtained results and discuss the potential applications.

1.4 Thesis Organization

This thesis has been arranged in the following way:

- In *Chapter 2*, the basic theory of SPP propagation has been described. This chapter introduces the fundamental knowledge and necessary mathematical formulations of SPP propagation at the single and double interface.
- In *Chapter 3*, the widely used models for modeling metals have been described in detail with necessary derivations. Since SPPs are created due to the coupling of photon energy to the free electrons of metal, modeling metals is one of the key steps for the simulation of SPP propagation.
- In *Chapter 4* we have developed our simulation model based on FDTD method. The fundamentals of the FDTD algorithm for 1D and 2D simulations are discussed with formulation of the “Absorbing Boundary Condition”. PML is introduced as a result to prevent the reflection at the boundary.
- In *chapter 5*, we have presented the modeling parameters of different optical materials using large scale nonlinear optimization method. The obtained modeling parameters and their validations are also provided in this chapter.
- In *Chapter 6*, we have used single pole-pair Lorentz model parameter of Arsenic Sulfide to simulate SPP propagation through optical nanostructure (dielectric-metal-dielectric waveguide). We have also investigated the electric and magnetic field profile and power transmission efficiency inside the nanostructure.
- In *Chapter 7*, we have provided the concluding remarks about our work and our future plans with the thesis

Chapter 2

SPP Propagation Theory

2.1 Introduction

Surface Plasmon Polariton (SPP) are infrared or visible frequency electromagnetic waves, which travel along a metal-dielectric or metal-air interface. Other words Surface plasmon polaritons are electromagnetic excitations propagating at the interface between a dielectric and a conductor, evanescently confined in the perpendicular direction. These electromagnetic surface waves arise via the coupling of the electromagnetic fields to oscillations of the conductor's electron plasma. So the term "*surface plasmon polariton*" explains that the wave involves both charge motion in the metal ("surface plasmon") and electromagnetic waves in the air or dielectric ("polariton"). SPPs can have tighter spatial confinement and higher local field intensity. Perpendicular to the interface. An SPP will propagate along the interface until its energy is lost due to absorption in the metal or scattering into other directions (such as into free space). If a photon is incident on a smooth metal surface, there is no SPP propagation at metal air surface due to the incompatibility that is comparable to internal reflection.

However, electromagnetic wave propagation is obtained from the solution of Maxwell's equations in each medium, and the associated boundary conditions. Maxwell's equations of macroscopic electromagnetism can be written as follows:

From Gauss's Law for the electric field

$$\nabla \cdot D = \rho_{ext} \quad (2.1)$$

From Gauss's Law for the magnetic field,

$$\nabla \cdot B = 0 \quad (2.2)$$

From Faraday's Law

$$\nabla \times E = -\frac{\partial B}{\partial t} \quad (2.3)$$

From Ampere's Law

$$\nabla \times H = J_{ext} + \frac{\partial D}{\partial t} \quad (2.4)$$

Here,

E is the electric field vector in volt per meter

D is the electric flux density vector in coulombs per square meter

H is the magnetic field vector in amperes per meter

B is the magnetic flux density vector in Webbers per square meter

ρ_{ext} is the charge density

J_{ext} is the current density

The four macroscopic fields can be also linked further via the polarization P and magnetization M by

$$D = \epsilon_o E + P \quad (2.5)$$

$$H = \frac{B}{\mu_o} - M \quad (2.6)$$

Now this equations can be simplified for linear, isotropic, nonmagnetic media as

$$D = \epsilon_o \epsilon_r E \quad (2.7)$$

$$B = \mu_o \mu_r H \quad (2.8)$$

where,

ϵ_o is electric permittivity of vacuum in Farad per meter

μ_o is the magnetic permeability of vacuum in Henry per meter

ϵ_r is the relative permittivity

μ_r is the relative permeability

Due to this field confinement and enhancement at a metal/dielectric interface, the SPP play a key role in various areas of science, such as optics, material science, and biology and very recently in nanoelectronics and nanophotonics.

Optical fibers and waveguides can carry information three order greater than their magnitude of interconnects but they have some limitations. Optical components can't be scaled down because diffraction destroy the propagation when light wave dimension is very small. An effective way to circumvent this drastic but natural limitation is to convert light into SPP waves, which can overcome the diffractive limit since the SPP wavelength is always very small; therefore, SPP devices are

called sub wavelength components. The incoming light will be thus converted into SPP and then processed (propagated at a remote location, focused, modulated, etc.) and reconverted at the output back into light with diffractive properties. In this way, by merging photonics and electronics at the nanoscale, plasmonic chips could be implemented for high data rate processing or very effective sensing applications.

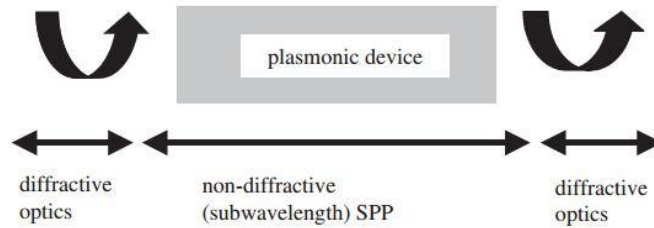


Figure. 2.1. Basic configuration of a plasmonic chip that use diffractive optics to excite the SPP and to outcouple the emitted light.

2.2 SPP at Single Interface

SPP propagation through metal-semiconductor surface is the simplest form of propagation at a single surface. Here, semiconductor has a positive dielectric constant and metal has a negative dielectric constant. For metal the bulk plasmon frequency will be ω and the amplitude decays perpendicular to the z - direction.

For the TM solutions in both spaces: metal and dielectric will be for $z > 0$

$$H_z(z) = A_2 e^{j\beta x} e^{-k_2 z} \quad (2.9)$$

$$E_x(z) = jA_2 \frac{1}{\omega \epsilon_0 \epsilon_2} k_2 e^{j\beta x} e^{-k_2 z} \quad (2.10)$$

$$E_z(z) = -A_1 \frac{\beta}{\omega \epsilon_0 \epsilon_2} e^{j\beta x} e^{-k_2 z} \quad (2.11)$$

And for $z < 0$

$$H_y(z) = A_1 e^{j\beta x} e^{-k_1 z} \quad (2.12)$$

$$E_x(z) = -jA_1 \frac{1}{\omega \epsilon_0 \epsilon_1} k_1 e^{j\beta x} e^{-k_1 z} \quad (2.13)$$

$$E_z(z) = -A_1 \frac{\beta}{\omega \epsilon_0 \epsilon_1} e^{j\beta x} e^{-k_1 z} \quad (2.14)$$

Here, as $A_1 = A_2$ and

$$\frac{k_2}{k_1} = -\frac{\epsilon_2}{\epsilon_1} \quad (2.15)$$

The surface wave exists at the metal dielectric interface with opposite sign of their real dielectric permittivity. So, we can write:

$$\beta = k_0 \sqrt{\frac{\epsilon_1 \epsilon_2}{\epsilon_1 + \epsilon_2}} \quad (2.16)$$

The TE surface mode can be expressed as:

$$E_y(z) = A_2 e^{j\beta x} e^{-k_2 z} \quad (2.17)$$

$$H_z(z) = -A_2 \frac{\beta}{\omega\mu_0} e^{j\beta x} e^{-k_2 z} \quad (2.18)$$

For $z > 0$

$$E_y(z) = A_1 e^{j\beta x} e^{-k_1 z} \quad (2.19)$$

$$H_x(z) = jA_1 \frac{1}{\omega\epsilon_0\epsilon_1} k_1 e^{j\beta x} e^{k_1 z} \quad (2.20)$$

$$H_z(z) = A_1 \frac{\beta}{\omega\epsilon_0\epsilon_1} e^{j\beta x} e^{k_1 z} \quad (2.21)$$

for $z < 0$. The continuity of E_y and H_x requires:

$$A_1(K_1 + K_2) = 0 \quad (2.22)$$

The surface requires that the real part of k_1 and k_2 should be greater than zero for confinement. This will be satisfied if $A_1 = A_2 = 0$. Therefore no surface modes for the TE polarization. SPP only exist for TM mode polarization.

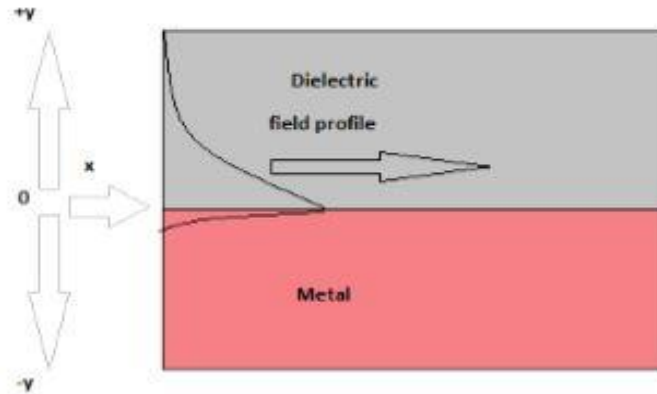


Figure 2.2: SPP at the single interface

2.3 SPP at Double Interface

Two mostly used double interface configurations of SPP waveguides are: Metal-Dielectric-Metal (MDM) and Dielectric-Metal-Dielectric (DMD). In these cases SPPs are formed on both interfaces. When the distance is shorter than decay distance, it forms coupled mode of SPP. This coupled mode of propagation can also be subdivided into even and odd modes, as shown in the figure

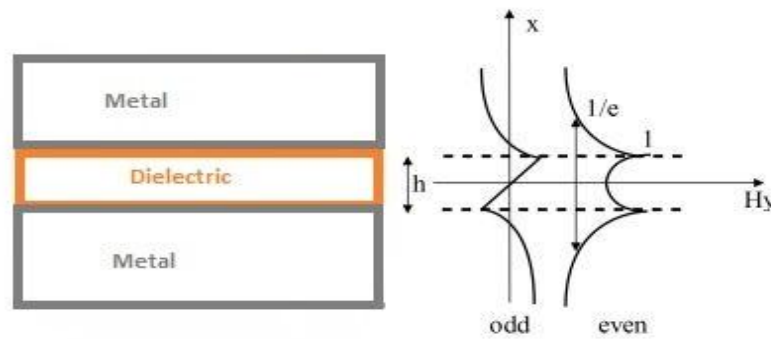


Figure 2.3: SPP at the double interface.

Chapter 3

Material Modeling Within Optical Range

3.1 Introduction

Low frequencies and long EM wavelengths metals are considered as perfect conductors. Perfect conductors have zero fields. At optical frequencies metals become dispersive materials rather than perfect conductors. It actually indicates that fields can exist inside metal which die very quickly inside metal. At frequencies higher than the optical range, metals become transparent or just dielectrics. In this chapter we study the properties of SPPs highly depending on the material response to light. Descriptions and derivations will be presented for various models describing the behavior of metal in the presence of light.

When an oscillating external electromagnetic field propagates inside any material, the materials behavior can be known from the following terms:

- ✓ D (electrical flux density)
- ✓ E (electric field intensity)
- ✓ P (polarization density)

For any material, the following equations apply [19]

$$D = \epsilon E \quad (3.1)$$

$$P = \epsilon_0 \chi E \quad (3.2)$$

$$D = \varepsilon_0 E + P \quad (3.3)$$

Where, ε is the permittivity in F/m and χ is the susceptibility which measures how easily it is polarized.

The relation n between permittivity and susceptibility is found by,

$$D = \varepsilon_0 E + \chi E \quad (3.4)$$

$$\text{Or, } D = \varepsilon_0 (E + \chi) \quad (3.5)$$

Combining equation 3.5 and 3.1 gives, in frequency domain,

$$\varepsilon(\omega) = \varepsilon_0 (1 + \chi(\omega)) \quad (3.6)$$

Thus we get relative permittivity as,

$$\varepsilon_r(\omega) = (1 + \chi(\omega)) \quad (3.7)$$

Permittivity and susceptibility of dispersive materials depend on frequency.

3.2 Different Material Models

3.2.1 The Debye Model

Materials are made of electric dipoles, so when an electric field is applied, these dipoles follow the coordination of the applied field with some relaxation time.

Electric field oscillating at a slow frequency \Rightarrow Strong polarization \Rightarrow Short relaxation time

Electric field oscillating at a fast frequency \Rightarrow Low polarization \Rightarrow long relaxation time

Polarization takes time to follow the electric field. At steady state, it is given by,

$$\dot{P}(t) = P_{\infty} - \tau \frac{dP(t)}{dt} \quad (3.8)$$

Where,

P_{∞} =polarization

$P(t)$ =instantaneous polarization

τ =relaxation time constant

$$P(t) = P_{\infty} (1 - e^{-t/\tau}) \quad (3.9)$$

Derivation of P(t) gives,

$$\frac{dP(t)}{dt} = \frac{1}{\tau} P_{\infty} e^{-t/\tau} \quad (3.10)$$

Substitution in equation (3.9),

$$.P(t) = P_{\infty} - \tau \frac{dP(t)}{dt} \quad (3.11)$$

P_{∞} is equal to the steady state value of permittivity which gives,

$$.P(t) = \varepsilon_0(\varepsilon - 1)E_{\infty} - \tau \frac{dP(t)}{dt} \quad (3.12)$$

Solving for E(t)

$$.\varepsilon_0(\varepsilon - 1)E(t) = P(t) + \tau \frac{dP}{dt} \quad (3.13)$$

Taking the equation to the frequency domain gives,

$$\varepsilon_0(\varepsilon - 1)E(\omega) = P(\omega)(1 + j\omega\tau) \quad (3.14)$$

Dividing by $\varepsilon_0 E(\omega)$ gives,

$$\frac{\varepsilon - 1}{(1 + j\omega\tau)} = \frac{P(\omega)}{\varepsilon_0 E(\omega)} = \chi(\omega), \quad (3.15)$$

where $\chi(\omega)$ is a complex-valued, frequency-domain susceptibility function which has one or more real poles at separate frequencies. Thus, the permittivity is given by,

$$.\varepsilon_r(\omega) = \chi(\omega) + 1 = \frac{\varepsilon - 1}{(1 + j\omega\tau)} + 1 \quad (3.16)$$

Conditions: For permittivity functions to fit in the range from 0 frequency to infinity frequency

$$\varepsilon(0) = \varepsilon_s, \varepsilon_r(\infty) = \varepsilon_\infty$$

where, ε_∞ is the permittivity at infinity frequency and ε_s is the static permittivity at DC.

Therefore the relative permittivity relation becomes,

$$\varepsilon_r(\omega) = \varepsilon_\infty + \frac{\varepsilon_s - \varepsilon_\infty}{1 + j\omega\tau} \quad (3.17)$$

For a Debye medium having P poles, we express the permittivity relation as,

$$\varepsilon_r(\omega) = \varepsilon_\infty + \sum_{p=1}^P \frac{\varepsilon_s - \varepsilon_\infty}{1 + j\omega\tau} = \varepsilon_\infty + \sum_{p=1}^P \frac{\Delta\varepsilon_p}{1 + j\omega\tau} \quad (3.18)$$

3.2.2 The Lorentz Model

In Lorentz model electrons are considered to be attached to atoms. They do not move freely in the metal. It's a heavy massed ball is connected to a small massed ball. There is restoring force acting between them which can be denoted by F_r

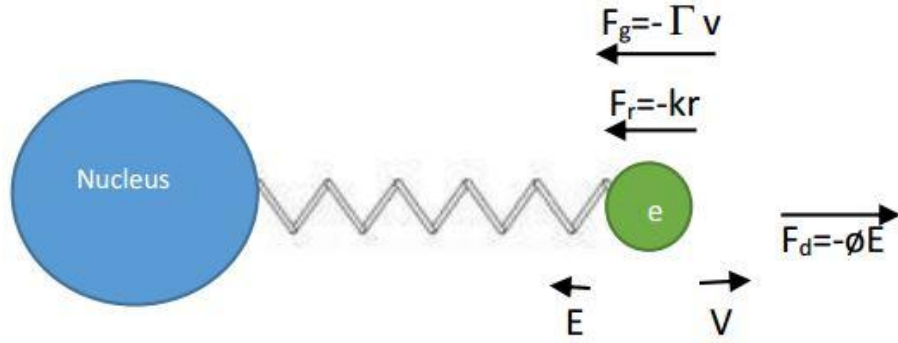


Figure 3.1: Forces acting in Lorentz model

The restoring force is given by

$$F_r = -kr \quad (3.19)$$

Where, k is spring constant in Newton per meter.

Therefore, Newton's first law of motion,

$$mr'' = -eE + \Gamma r \quad (3.20)$$

becomes,[20]

$$mr'' + m\Gamma r + mkr + eE = 0 \quad (3.21)$$

Defining the natural frequency $\omega_0 = \sqrt{\frac{k}{m}}$, in frequency domain the above equation will be,

$$R(\omega)(m\omega_0^2 + jm\omega\Gamma - m\omega^2) + eE(\omega) = 0 \quad (3.22)$$

The polarization for n electrons is given by

$$.P(\omega) = -neR(\omega) \quad (3.23)$$

From equations (3.23) and (3.24), we find,

$$.P(\omega) = \frac{ne^2}{m(j\Gamma\omega - \omega^2)} E(\omega) \quad (3.24)$$

Dividing by $\varepsilon_0 E$ we get, susceptibility $\chi(\omega)$

$$\frac{P(\omega)}{\varepsilon_0 E\omega} = \frac{ne^2}{\varepsilon_0 m(\omega_0^2 + j\Gamma\omega - \omega^2)} = \chi(\omega) \quad (3.25)$$

From $D(\omega) = \varepsilon_0 E(\omega)(1 + \chi(\omega))$ we get D in frequency domain as

$$D(\omega) = \varepsilon_0 \left(1 + \frac{\omega_p^2}{\omega_0^2 + j\Gamma\omega - \omega^2}\right) E(\omega) \quad (3.26)$$

For multiple pole P' the Lorentz model looks like,

$$\varepsilon(\omega) = \varepsilon_\infty + \sum_{p=1}^{p'} \frac{\Delta\varepsilon_p \omega_p^2}{\omega_p^2 + 2j\omega\gamma_p - \omega^2} \quad (3.27)$$

Where, $\Delta\varepsilon = \varepsilon_s - \varepsilon_\infty$ is the change in relative permittivity due to the Lorentz pole pair, ω_p is the frequency of the pole pair and γ_p is the damping coefficient.

3.2.3 Modified Lorentz Model

To obtain more accurate fitting, Lorentz Model is modified[21] as follows:

$$\varepsilon(\omega) = \varepsilon_\infty + \sum_{p=1}^p \Delta\varepsilon_p \frac{(\omega_p^2 - i\gamma_p' \omega)}{\omega_p^2 - 2i\omega\gamma_p - \omega^2} \quad (3.28)$$

$$\Delta\varepsilon_p = \varepsilon_s - \varepsilon_\infty \quad (3.29)$$

where, ε_∞ is permittivity at infinite frequency, ω_p is the pole-pair frequency, γ_p is the damping coefficient, $\Delta\varepsilon_p$ is the change in relative permittivity due to change in p th pole and ε_s is zero frequency relative permittivity. Here, ω_p , γ_p , γ_p' are in $1/\mu\text{m}$.

3.3 Material Dispersion

Material dispersion is a phenomenon in which different optical wavelengths propagate at different velocities, depending on the refractive index of the material used. The phase velocity of numerical wave modes can differ from C by an amount varying with wavelength, propagation direction and grid discretization. Propagation of a plane wave is fully described by two quantities: the optical frequency $\omega = 2\pi f$ and the wave vector \vec{k} . The direction of \vec{k} determines the direction of propagation of the plane wave. We know the phase velocity is,

$$v = \frac{c}{n} = \frac{1}{\sqrt{\mu\varepsilon}} \quad (3.31)$$

Where, n is the refractive index and c is velocity of light in free space.

Sometimes, K is called wavenumber, which is

$$k = \frac{2\pi}{\lambda} \quad (3.32)$$

The wave equation of dispersion less media is free of ω and k and we ended up with an equation

$$\frac{\partial^2 \psi}{\partial t^2} = v^2 \frac{\partial^2 \psi}{\partial x^2} \quad (3.33)$$

Solving this equation with the help of exponential function $\psi(x, t) = Ae^{i(kx - \omega t)}$ we get the solution as,

$$\omega^2 = v^2 k^2 \quad (3.34)$$

The velocity of the wave is

$$v = \pm \frac{\omega}{k}$$

$$\text{Or, } k = \pm \frac{\omega}{v} \quad (3.35)$$

Where, (+) sign means the $-x$ direction propagation and (-) means $+x$ direction propagation. We can find our expected parameters from this v which relates with equation (3.31). The magnetic flux density and electric flux density for dispersive medium are:

$$\bar{D} = \epsilon \bar{E} \quad (3.36)$$

$$\bar{B} = \mu \bar{H} \quad (3.37)$$

Chapter 4

Overview of Finite-Difference Time Domain Method

4.1 The Yee Algorithm

The Finite-Difference Time Domain (FDTD) method is one of the most popular method solving electromagnetic problems (Maxwell's equation). It can cover a wide frequency range with single simulation run. Its charming property is that it can deal with a non-linear material in linear way. To understand a wave propagation simulation FDTD is preferred most. This method was first proposed by Yee in 1966 [22].

To solve an electromagnetic problem, the idea is to simply discretize the Maxwell's equation with central difference approximation both in space and time. At first, we have allocate the electric and magnetic field components in space and then let them march in time for the evaluation.

Maxwell's equation actually consist of 4 basic set of equations. They are as follows:

$$\text{Gauss's Law} : \nabla \cdot \bar{D} = \rho_v \quad (4.1)$$

$$\text{Gauss's Law for Magnetism} : \nabla \cdot \bar{B} = 0 \quad (4.2)$$

$$\text{Faraday's Law} : \nabla \times \bar{E} = -\frac{\partial \bar{B}}{\partial t} \quad (4.3)$$

$$\text{Ampere's Law: } \nabla \times \vec{H} = \vec{J} + \frac{\partial \vec{D}}{\partial t} \quad (4.4)$$

We will not use the two Gauss' laws (4.1) and (4.2) since they can be derived from the curl equations (4.3) and (4.4). In linear isotropic non-dispersive materials, we have the following definitions for the electric displacement (\mathbf{D}) and magnetic flux (\mathbf{B}):

$$D = \varepsilon E = \varepsilon_r \varepsilon_0 E \quad (4.5)$$

$$B = \mu H = \mu_r \mu_0 H \quad (4.6)$$

The Time dependent Maxwell's curl equations in the free space is:

$$\frac{\partial \vec{H}}{\partial t} = -\frac{1}{\mu} \nabla \times \vec{E} \quad (4.7)$$

$$\frac{\partial \vec{E}}{\partial t} = \frac{1}{\varepsilon} \nabla \times \vec{H} \quad (4.8)$$

Now, considering the Taylor series expansion of the function $f(x)$ expanded about the point x with an offset of $(\pm\Delta x)$ which gives two other functions $f(x+\Delta x)$ and $f(x-\Delta x)$. Subtracting these two functions and dividing by distance $(2\Delta x)$ gives the central-difference approximation.

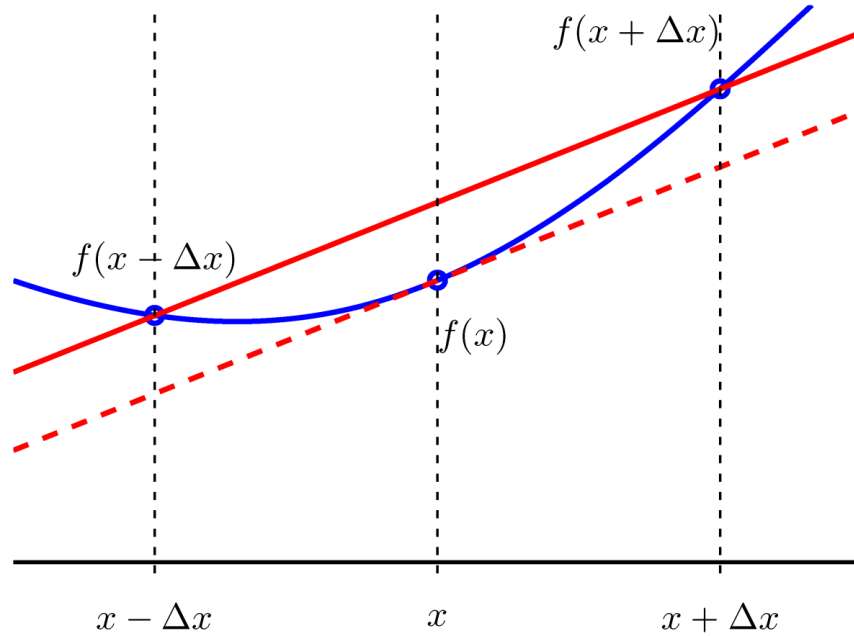


Figure 4.1: Estimation for the derivative of $f(x)$ using Forward, Backward and Central-Difference

$$\frac{df(x)}{dx} = f'(x) \cong \frac{f(x + \Delta x) - f(x - \Delta x)}{2\Delta x} \quad (4.9)$$

To solve Maxwell's equation numerically, we evaluate Faraday's Law and in the Cartesian co-ordinate system to get three magnetic and electric field components H_x , H_y , H_z and E_x , E_y , E_z respectively. The curl operation of the equations (4.2)&(4.3) produces these six coupled scalar equations:

From Faraday's Law:

$$\frac{\partial H_x}{\partial t} = \frac{1}{\mu} \left(\frac{\partial E_y}{\partial z} - \frac{\partial E_z}{\partial y} \right) \quad (4.10)$$

$$\frac{\partial H_y}{\partial t} = \frac{1}{\mu} \left(\frac{\partial E_z}{\partial x} - \frac{\partial E_x}{\partial z} \right) \quad (4.11)$$

$$\frac{\partial H_z}{\partial t} = \frac{1}{\mu} \left(\frac{\partial E_x}{\partial y} - \frac{\partial E_y}{\partial x} \right) \quad (4.12)$$

From Ampere's law:

$$\frac{\partial E_x}{\partial t} = \frac{1}{\varepsilon} \left(\frac{\partial E_z}{\partial y} - \frac{\partial E_y}{\partial z} \right) \quad (4.13)$$

$$\frac{\partial E_y}{\partial t} = \frac{1}{\varepsilon} \left(\frac{\partial E_x}{\partial z} - \frac{\partial E_z}{\partial x} \right) \quad (4.14)$$

$$\frac{\partial E_z}{\partial t} = \frac{1}{\varepsilon} \left(\frac{\partial E_y}{\partial x} - \frac{\partial E_x}{\partial y} \right) \quad (4.15)$$

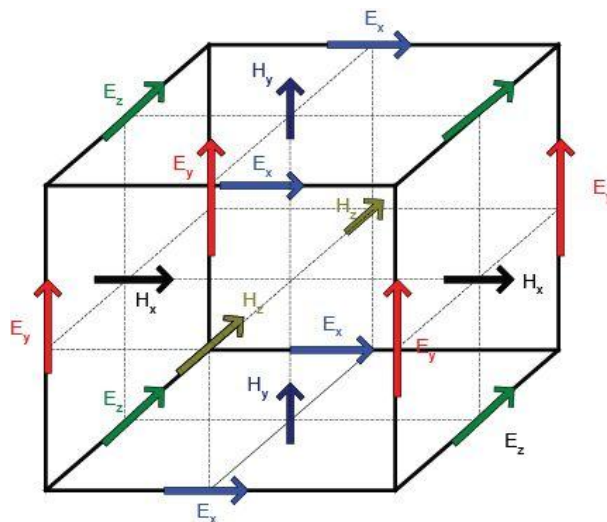


Figure 4.2: Yee's spatial grid showing electrical and magnetic field component per cell.

4.1.1 One-Dimensional Simulation

For one dimensional z-directed TEM wave ($H_z = E_z = 0$) with no variation in the X and Y direction (i.e. $\frac{\partial}{\partial y} = \frac{\partial}{\partial x} = 0$), those 6 equations become:

$$\frac{\partial E_x}{\partial t} = -\frac{1}{\epsilon} \frac{\partial H_y}{\partial z} \quad (4.16)$$

$$\frac{\partial H_y}{\partial t} = -\frac{1}{\mu} \frac{\partial H_x}{\partial z} \quad (4.17)$$

Now replacing all the derivatives in Ampere's and Faraday's laws with central-difference approximation from equation (4.1) and discretize in space and time, we get

$$\frac{\partial E_x(z, t)}{\partial t} = \frac{E_x^{n+1/2}(k) - E_x^{n-1/2}(k)}{\Delta t} \quad (4.18)$$

$$\frac{\partial H_y(z, t)}{\partial z} = \frac{H_y^n(k+1/2) - H_y^n(k-1/2)}{\Delta x} \quad (4.19)$$

Solving these resulting difference equations we obtain "Update equations" that express the future fields (known) in terms of past fields (unknown).

$$E_x^{n+1/2}(k) = E_x^{n-1/2}(k) - \frac{\Delta t}{\epsilon_0 \cdot \Delta x} [H_y^n(k+1/2) - H_y^n(k-1/2)] \quad (4.20)$$

$$H_y^{n+1}(k+1/2) = H_y^n(k+1/2) - \frac{\Delta t}{\mu_0 \cdot \Delta x} \left[E_x^{n+1/2}(k+1) - E_x^{n+1/2}(k) \right] \quad (4.21)$$

Actually the solution is made by Leap-Frog method, which will be discussed later.

4.1.2 Two-Dimensional Simulation

The structures studied in this project are one-dimensional metallic thin films (with or without surface corrugations) which can be described in the two-dimensional space. The number of FDTD relations can thus be reduced from six in the 3D space to only three in 2D. There are two sets of three fields which can be used. They are designated as the TM_z and TE_z modes, respectively corresponding to the sets of field components (E_z, H_x, H_y) and (H_z, E_x, E_y) . It is important to distinguish the TE/TM FDTD modes from the TE/TM polarization modes. The former denotes two independent sets of electromagnetic field components in the 2D space; while the latter designates the fundamental two independent linear polarization modes of light relatively to the plane of incidence. In our FDTD algorithm, we have implemented the TE_z FDTD mode in order to model a TM-polarization incidence on the structure.

For the Transverse Electric (TE) or Transverse Magnetic (TM) in 2D space, if no variation in Z-direction ($\frac{\partial}{\partial z} = 0$), Maxwell's equations look like

$$\frac{\partial E_x}{\partial t} = \frac{1}{\varepsilon} \frac{\partial H_z}{\partial y} \quad (4.22)$$

$$\frac{\partial E_y}{\partial t} = -\frac{1}{\varepsilon} \frac{\partial H_z}{\partial x} \quad (4.23)$$

$$\frac{\partial E_x}{\partial t} = \frac{1}{\mu} \left(\frac{\partial E_x}{\partial y} - \frac{\partial E_y}{\partial x} \right) \quad (4.24)$$

Now we have to discretize these equations first,

$$\frac{\partial E_x}{\partial t} = \frac{1}{\varepsilon} \frac{H_z(i, j) - H_z(i, j-1)}{\Delta y} \quad (4.25)$$

$$\frac{\partial E_y}{\partial t} = -\frac{1}{\varepsilon} \frac{H_z(i, j) - H_z(i-1, j)}{\Delta x} \quad (4.26)$$

$$\frac{\partial H_z}{\partial t} = \frac{1}{\mu} \left(\frac{E_x(i, j+1) - E_x(i, j)}{\Delta y} - \frac{\partial E_y(i+1, j) - \partial E_y(i, j)}{\Delta x} \right) \quad (4.27)$$

Therefore the previous set of equations become,

$$\frac{E_x^n(i, j) - E_x^{n-1}(i, j)}{\Delta t} = \frac{1}{\varepsilon} \frac{H_z^{n-1/2}(i, j+1/2) - H_z^{n-1/2}(i, j-1/2)}{\Delta y} \quad (4.30)$$

$$\frac{E_y^n(i, j) - E_y^{n-1}(i, j)}{\Delta t} = -\frac{1}{\varepsilon} \frac{H_z^{n-1/2}(i+1/2, j) - H_z^{n-1/2}(i-1/2, j)}{\Delta x} \quad (4.31)$$

$$\frac{H_y^{n+1/2}(i, j) - H_y^{n-1/2}(i, j)}{\Delta t} = \frac{1}{\mu} \left(\frac{E_x^n(i, j+1/2) - E_x^{n-1/2}(i, j-1/2)}{\Delta y} - \frac{\partial E_y^n(i, j+1/2) - \partial E_y^n(i-1/2, j)}{\Delta x} \right) \quad (4.32)$$

After implementing the leap in space, we implement a leap in time. Now the update equations become,

$$E_x^n(i, j) = E_x^{n-1}(i, j) + \frac{\Delta t}{\varepsilon} \frac{H_z^{n-1/2}(i, j+1/2) - H_z^{n-1/2}(i, j-1/2)}{\Delta y} \quad (4.33)$$

$$E_y^n(i, j) = E_y^{n-1}(i, j) - \frac{\Delta t}{\varepsilon} \frac{H_z^{n-1/2}(i+1/2, j) - H_z^{n-1/2}(i-1/2, j)}{\Delta x} \quad (4.34)$$

$$H_z^{n+1/2}(i, j) = H_z^{n-1/2}(i, j) + \frac{\Delta t}{\mu} \left(\frac{E_x^n(i, j+1/2) - E_x^n(i, j-1/2)}{\Delta y} - \frac{E_y^n(i+1/2, j) - E_y^n(i, j-1/2)}{\Delta x} \right) \quad (4.35)$$

Using the leap frog method we continue to update our equations. The term “n+1” means one time step later and “k” means the distance $z=\Delta x.k$. E and H are both interleaved in space and time. H uses the arguments $k+1/2$ and $k-1/2$ to indicate that H field values are assumed to be located between E field values.

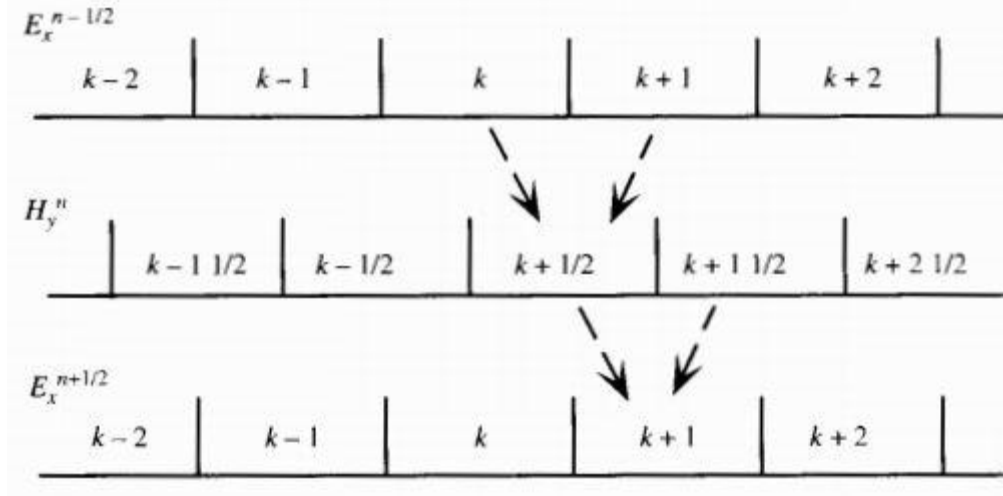


Figure 4.3: Updating Field values using Leap Frog method

4.2 Stability

A classical electromagnetic wave propagating in free space cannot travel faster than the speed of light. In FDTD, this condition is mathematically expressed by the *Courant condition* which determines the suitable size range of Δx and Δt , respectively the space and time discretization steps. This is also known as “Stability Condition”. To propagate a distance of one cell requires a minimum time of $\Delta t = \Delta x / c_0$. For two dimensional simulation, we need to allow propagation in the diagonal direction. Then $\Delta t = \Delta x / \sqrt{2}c_0$ and similarly for three dimensional $\Delta t = \Delta x / \sqrt{3}c_0$. We can summarize by the following relation,

$$\Delta t = \Delta x / \sqrt{nc_0} \quad (4.36)$$

Where ‘n’ is dimension of the simulation. If no dimension is specified, for simplicity we use,

$$\Delta t = \frac{\Delta x}{2c_0} \quad (4.37)$$

4.3 Absorbing Boundary Condition

When simulating propagation of EM waves, it is necessary to keep unwanted reflections from coming back and the computational domain needs to be terminated. Terminating the computational domain for a medium surrounded by metals or perfect electric conductors is achieved by forcing the fields to be equal to zero. It is necessary to keep unwanted reflections from coming back and Probably the best solution is the *Perfectly Matched Layer* (PML), proposed by Berenger, which absorbs outgoing wave. Berenger introduced two quantities, σ and σ^* , which are the electric conductivity and magnetic conductivity. The resulting equations for TE waves inside the PML are given by

$$\epsilon_0 \frac{\partial E_x}{\partial t} + \sigma E_x = \frac{\partial H_x}{\partial y} \quad (4.38)$$

$$\epsilon_0 \frac{\partial E_y}{\partial t} + \sigma E_y = -\frac{\partial H_z}{\partial x} \quad (4.39)$$

$$\mu_0 \frac{\partial H_z}{\partial t} + \sigma^* H_z = \frac{\partial E_x}{\partial y} - \frac{\partial E_y}{\partial x} \quad (4.40)$$

When the impedance of two media are equal, then no reflection occurs at normal incidence when the wave travels from one medium to another, which is known as impedance matching and this is applied in PML. This condition results in the following equation.

$$\frac{\sigma}{\epsilon_0} = \frac{\sigma^*}{\mu_0} \quad (4.41)$$

The problem is solved for normal incidence only. However, the algorithm should deal with all forms of incidence. Therefore, we should split the field H_z into two fields H_{zx} and H_{zy} where one is at normal incidence and the other is tangential to the PML and their summation is equal to H_z . Applying this to the FDTD means splitting σ_x to σ_x^* and σ_y^* where the first deals with H_{zy} and the other deals with H_{zx} . Thus we get three equations:

$$\mu_0 \frac{\partial H_{zx}}{\partial t} + \sigma_x^* H_{zx} = -\frac{\partial E_y}{\partial x} \quad (4.42)$$

$$\mu_0 \frac{\partial H_{zy}}{\partial t} + \sigma_y^* H_{zy} = -\frac{\partial E_x}{\partial y} \quad (4.43)$$

$$H_z = H_{zx} + H_{zy} \quad (4.44)$$

In the computational domain for TE mode, we have σ_x, σ_y and σ_y^* equal to zero, but they are generally non-zero inside the PML. Applying PML in this manner works well with a homogeneous medium. However, problems are caused by objects that reach the limits of the simulation space and the presence of dispersive material and non-dispersive material at the PML walls. Zaho introduced a PML algorithm that is material-independent and he called it material-independent PML (MIPML). The

main idea is to apply the PML algorithm on a layer different than the layer of electric and magnetic fields.

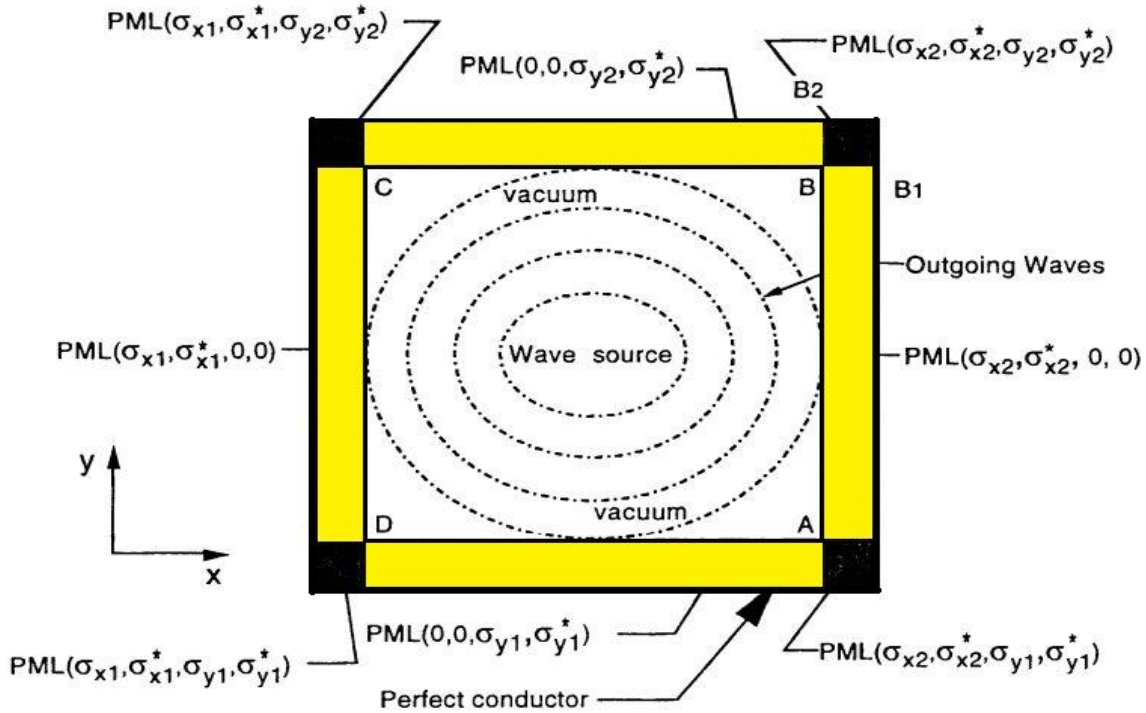


Figure 4.4: PML setup

The problem is that, if the PML is applied on E and H fields, then the constants in the loops involved with E and H are affected by the material in the simulation space. It is difficult to produce constants that take care of material inside the simulation space and PML walls. Therefore, in the MIPML, the constants involved with electric flux density D and magnetic flux density B (which are material independent by their nature) are responsible for the PML walls only. Therefore, the new electric conductivity, σ and magnetic conductivity, σ^* are introduced in Maxwell's equations.

The following two-dimensional simulation shows the radiation from a Gaussian pulse given at the middle of the mater. The radiation is absorbed by the PML and it is demonstrated in the following figures:

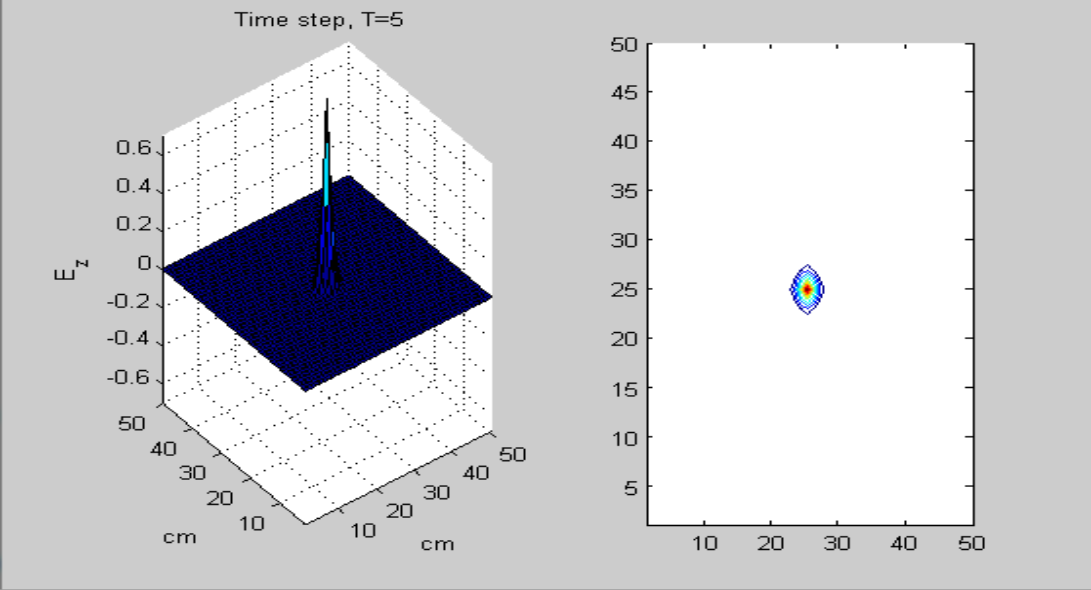


Figure 4.5: Propagation of electric field at time step, T= 5

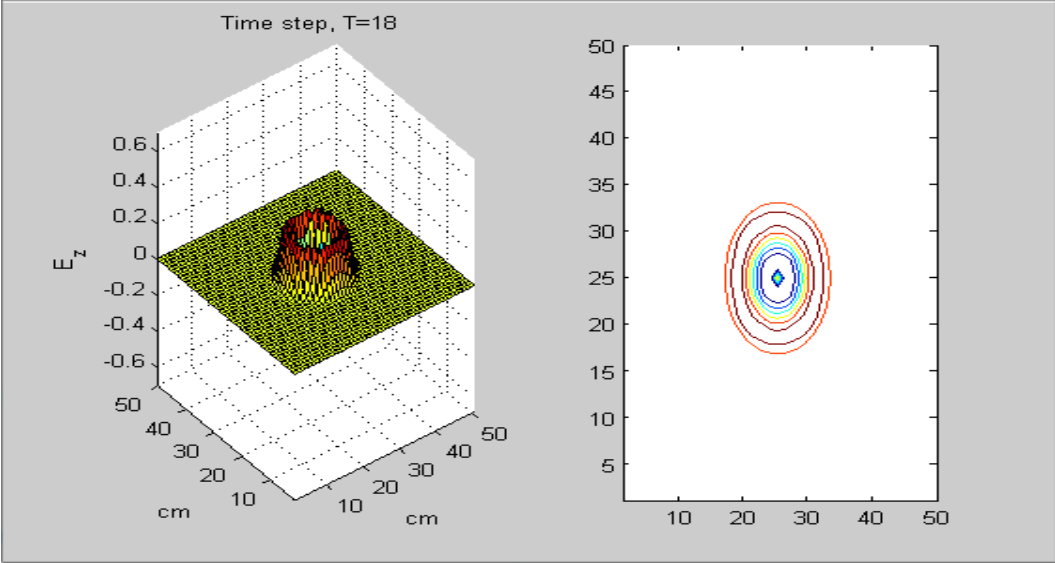


Figure 4.6: Propagation of electric field at time step, T=18

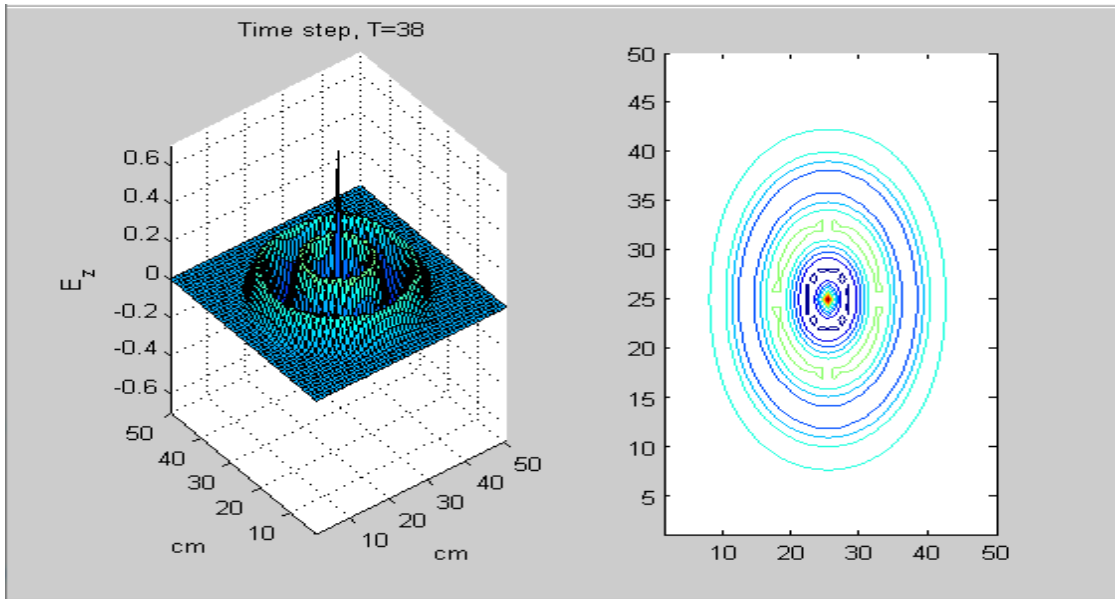


Figure 4.7: Propagation of electric field at time step, $T=38$

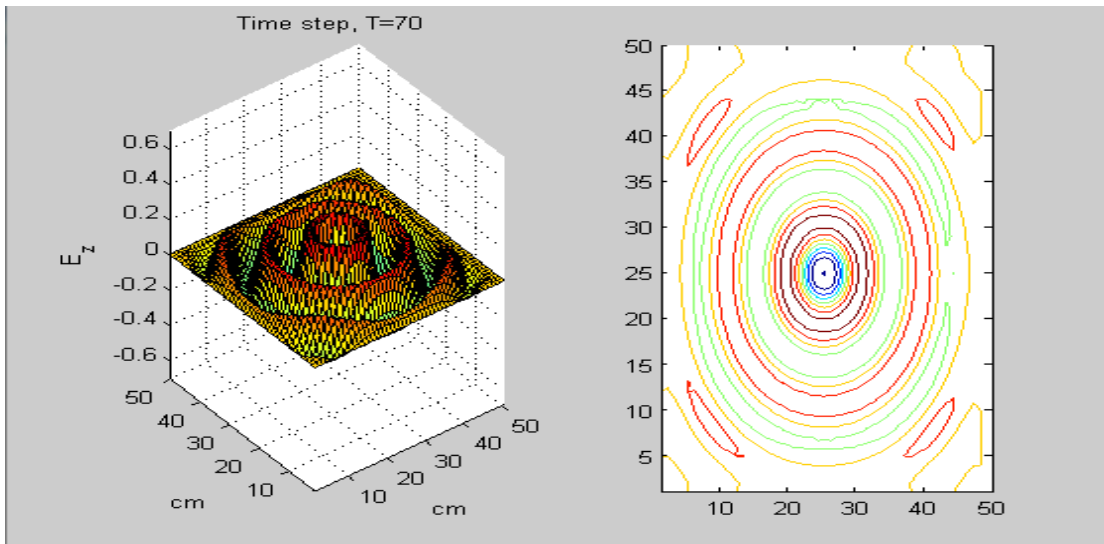


Figure 4.8: Propagation of electric field at time step, $T=70$

4.4 Material Dispersion in the FDTD

Modeling metals in FDTD requires knowledge of modeling dispersive materials. Three main methods used to model dispersive materials:

1. The ADE Method [23]
2. Z-Transformation [24, 25]
3. Recursive Convolution(RC) Method [26]

For optimization purpose we used ADE method as it is more straightforward to handle non-linear dispersive materials than RC method. So we will discuss about ADE FDTD method while Z-transformation and RC will be briefed also.

4.4.1 The Auxiliary Differential Equation (ADE)

To introduce dispersion relation in FDTD, Taflove proposed ‘Auxiliary Differential Equation’. It actually use Fourier transform to convert dispersion relation from frequency domain to time domain. The Fourier transform results in a relationship between the new E field value and the previous E and D values. This relation can be added to the algorithm to update the E fields. The new algorithm with ADE becomes

$$\frac{\partial H_z}{\partial t} = -\frac{1}{\mu} \left(\frac{\partial E_x}{\partial y} - \frac{\partial E_y}{\partial x} \right) \quad (4.45)$$

$$\frac{\partial D_x}{\partial t} = \frac{\partial H_z}{\partial y} \quad (4.46)$$

$$E = f(D, E) \quad (4.47)$$

As an example, we will explain how to get the function relating D to E in a dispersive medium. Starting with

$$D(\omega) = \varepsilon_0 \frac{\sigma}{j\omega} E(\omega) \quad (4.48)$$

Multiplying by $j\omega$

$$j\omega D(\omega) = \varepsilon_0 \sigma E(\omega) \quad (4.49)$$

Applying the Fourier transform

$$\frac{dD(t)}{dt} = \varepsilon_0 \sigma E(t) \quad (4.50)$$

Discretizing using forward difference scheme

$$\frac{D^n - D^{n-1}}{\Delta t} = \varepsilon_0 \sigma E^n \quad (4.51)$$

Finally, solving for E

$$E^n = \frac{D^n - D^{n-1}}{\varepsilon_0 \sigma \Delta t} \quad (4.52)$$

4.4.2 Z-Transformation

Z-transformation is very useful when dealing with functions in the sampled time domain. In FDTD the fields are already in discrete form and they need to be processed through a frequency-dependent system (permittivity or permeability). Actually this method is similar like ADE except the fact that it is simple and short. The transform from the frequency domain to the Z-domain is done as follows:

$$D(\omega) = \varepsilon(\omega)E(\omega) \Leftrightarrow D(z) = \varepsilon(z)\Delta t E(z) \quad (4.53)$$

where $\varepsilon(z)$ is z-transform of $\varepsilon(\omega)$ as an example, as already done in the ADE. The relation between D and E is given by

$$D(\omega) = \varepsilon_0 \frac{\sigma}{j\omega} E(\omega) \quad (4.54)$$

Applying Z-transform,

$$D(z) = \frac{\varepsilon_0 \sigma}{1-z^{-1}} \Delta t E(z) \quad (4.55)$$

Multiplying by $(1-z^{-1})$

$$D(z)(1-z^{-1}) = \varepsilon_0 \sigma E(z) \quad (4.56)$$

Or

$$D(z) - z^{-1}D(z) = \varepsilon_0 \sigma \Delta t E^n \quad (4.57)$$

Going from the z-domain to the time-domain

$$D^n - D^{n-1} = \varepsilon_0 \omega \Delta t E^n \quad (4.58)$$

Finally, solving for E

$$E^n = \frac{D^n - D^{n-1}}{\varepsilon_0 \sigma \Delta t} \quad (4.59)$$

which matches with ADE.

4.4.3 Recursive Convolution

Luebbers et al. formulated the first frequency dispersive FDTD algorithm using the recursive convolution (RC) scheme. Later it became piecewise linear recursive convolution (PLRC) method for more precision [27]. Due to the accuracy and stability [28] this method is more suitable than any other method. The numerical dispersion caused by the permittivity varies with space has significant value. The dispersion relation is shown in Ai et al. [29]. In the initial derivation of PLRC method for a linear dispersive medium, the relation between electric flux density and electric field intensity is expressed as:

$$D(t) = \varepsilon_0 \varepsilon_\infty E(t) + \varepsilon_0 \int_0^t E(t-\tau) \chi(\tau) d\tau \quad (4.60)$$

which can be discretized as:

$$D^n = \varepsilon_0 \varepsilon_\infty E^n + \varepsilon_0 \int_0^{n\Delta t} E(n\Delta t - \tau) \chi(\tau) d\tau \quad (4.61)$$

Chapter 5

Parameter Optimization of Optical Materials

The optimized Lorentz Model (LM) parameter of three materials and Modified Lorentz Model (MLM) parameters for another nine materials are presented. A large scale non-linear algorithm has been used for the optimization of optical parameters. The optimized parameters are used to determine the complex relative permittivity of these ten materials in optical and IR region of electromagnetic spectrum. The complex relative permittivity obtained, is compared with the experimental data. The comparison shows an excellent agreement.

5.1 Material Models

5.1.1 Lorentz Model

Lorentz media are characterized by a complex valued, frequency domain susceptibility function $\chi(\omega)$ that has one or more pairs of complex poles. For a Lorentz medium characterized by a single pole pair, we have

$$\chi_p(\omega) = \frac{\Delta\epsilon\omega_p^2}{\omega_p^2 - 2i\omega\gamma_p - \omega^2} \quad (5.1)$$

Where, $\Delta\varepsilon$ is the change in relative permittivity due to Lorentz pole pair, ω_p is the frequency of the pole-pair and γ_p is the damping coefficient. The real valued time domain susceptibility function $\chi(t)$ is obtained by Fourier transformation of (5.1), which yields the exponentially decaying sinusoidal function

$$\chi_p(t) = \frac{\Delta\varepsilon_p \omega_p^2}{\sqrt{\omega_p^2 - \gamma_p^2}} e^{-\gamma_p t} \sin(\sqrt{\omega_p^2 - \gamma_p^2} t) U(t) \quad (5.2)$$

For a Lorentz medium of P pole pairs, the expression in (5.1) can be extended to express the relative permittivity as[11, 21]

$$\varepsilon(\omega) = \varepsilon_\infty + \sum_{p=1}^P \frac{\Delta\varepsilon \omega_p^2}{\omega_p^2 - 2i\omega\gamma_p - \omega^2} \quad (5.3)$$

where P is the number of pole-pair.

5.1.2 Modified Lorentz Model

The frequency dependent complex permittivity for P pole-pair modified Lorentz model[21] can be expressed as

$$\varepsilon(\omega) = \varepsilon_\infty + \sum_{p=1}^P \Delta\varepsilon_p \frac{(\omega_p^2 - i\gamma_p' \omega)}{\omega_p^2 - 2i\omega\gamma_p - \omega^2} \quad (5.4)$$

$$\Delta\varepsilon_p = \varepsilon_s - \varepsilon_\infty \quad (5.5)$$

where ϵ_∞ is the permittivity at infinite frequency, ω_p is the pole-pair frequency, γ_p is the damping coefficient, $\Delta\epsilon_p$ is the change in relative permittivity due to change in modified Lorentz pole-pair and ϵ_s is zero frequency relative permittivity. Here $\omega_p, \gamma_p, \gamma_p'$ are in $1/\mu m$ and speed of light is unity.

5.2 Optimized Materials

Optical parameter optimized for the tabulated material using Lorentz model and modified Lorentz model.

Material	Model Used
Crystalline Arsenic Sulfide	Lorentz Model
Yttrium Aluminum Garnet	
Silicon Carbide	
Copper	Modified Lorentz Model
Hexagonal Cobalt	
Iridium	
Nickel	
Palladium	
Platinum	
Titanium	

5.3 Optimization Method

In recent years, different approaches have been taken for modeling frequency dependent material properties in FDTD methods for electromagnetics. Among them recursive convolution (RC), Z-transformation and auxiliary differential equation (ADE) methods are most efficient [30]. Numerical methods used for non-linear optimization problems are iterative in nature [31]. The ADE method is more straightforward to handle non-linear dispersive materials, but it is not possible with RC due to the linearity intrinsic to the convolution integral. Moreover, the ADE method requires minor changes in the algorithm when modeling materials with different shapes of the permittivity function. That's why in this paper, we have used ADE technique for optimization purpose.

The experimental values of refractive index and extinction coefficient has been taken from the book of Edward D. Palik [32] and used them to obtain the complex relative permittivity for each material using the following equations:

$$\epsilon_{\text{experimental}}(\omega) = \epsilon_{\text{real}}(\omega) + i\epsilon_{\text{imag}}(\omega) \quad (5.6)$$

$$\epsilon_{\text{real}}(\omega) = n^2 - k^2 \quad (5.7)$$

$$\epsilon_{\text{imag}}(\omega) = 2nk \quad (5.8)$$

Where, n=refractive index and k=extinction coefficient.

The ADE algorithms have a much better numerical performance and can be used to extract any parameter of the equations (5.3) & (5.4) within a defined range. It has its

uses in image enhancement and noise filter too. This technique works as follows: first, we assume a value over a wide frequency range for our desired parameters; depending on that value output is obtained, then we move on to the next range. When the whole range is covered, an optimized value is obtained for every parameter.

Here, we defined a particular range for every parameter of the Lorentz model and modified Lorentz model. The constraint that we followed for the optimization of Lorentz and modified Lorentz parameters are $\varepsilon_{\infty} \geq 1$, $\varepsilon_s > \varepsilon_{\infty}$, $\gamma_p \geq 1$ and $\gamma_p' \geq 1$. Then we keep updating the parameters value within that range until the RMS deviation reaches the desired level. If the RMS deviation is still not less than our desired value, then we again define the range newly and keep the iterations going on. Thus we obtain the optimized complex relative permittivity with minimum RMS deviation through an iterative method. Here, we calculated the RMS deviation by using the following equation:

$$\text{RMS-deviation} = \sqrt{\frac{\sum_{n=1}^N \varepsilon_{n(\text{experimental})}^2(\omega) - \sum_{n=1}^N \varepsilon_{n(\text{optimized})}^2(\omega)}{\sum_{n=1}^N n}} \quad (5.9)$$

5.4 Optimized parameters

5.4.1 Optimized parameter for Dielectric material for Lorentz model

Table 5.1: Optimized parameter for Crystalline Arsenic Sulfide, Yttrium Aluminum Garnet, Silicon Carbide for Lorentz model

Material	Parameters								
	Wavelength μm	ϵ_{∞}	$\epsilon(\omega)$	No. of pole	$\Delta\epsilon$	ω_p	γ_p	γ_p'	RMS Deviation
As ₂ S ₃	0.58-1.35	1.000010	8.627+ 1.16e-11i	01	7.291255	0.003577	0.000000	-	0.25358
Y ₃ Al ₅ O ₁₂	0.20-1.40	1.000000	3.298+4.195i	01	2.277736	0.008875	0.000000	-	0.00305
SiC	0.49-2.00	1.000000	6.630+ 2.418e-6i	01	5.531084	0.006033	0.000000	-	0.01006

The optimized parameters for three dielectric materials using large scale non-linear algorithm are presented on Table 5.1. In each case only single Lorentz pole pair is used. From the table it is seen that RMS deviation between the experimental data and fitted data is very small which indicates the robustness and accuracy of the optimization algorithm.

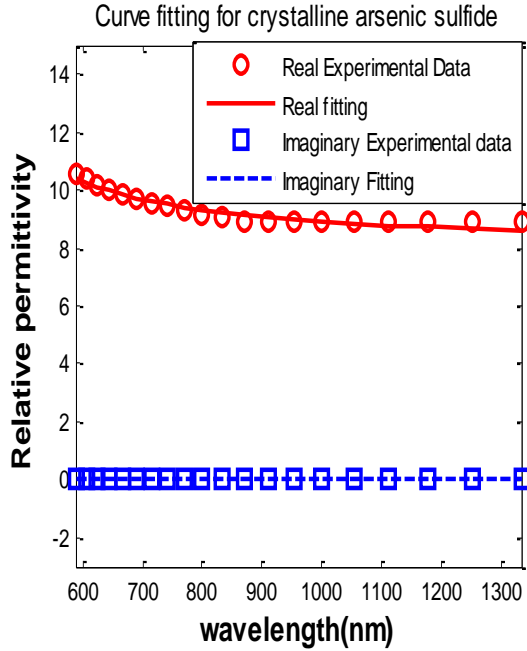


Figure 5.1: Curve fitting for Crvstalline Arsenic Sulfide

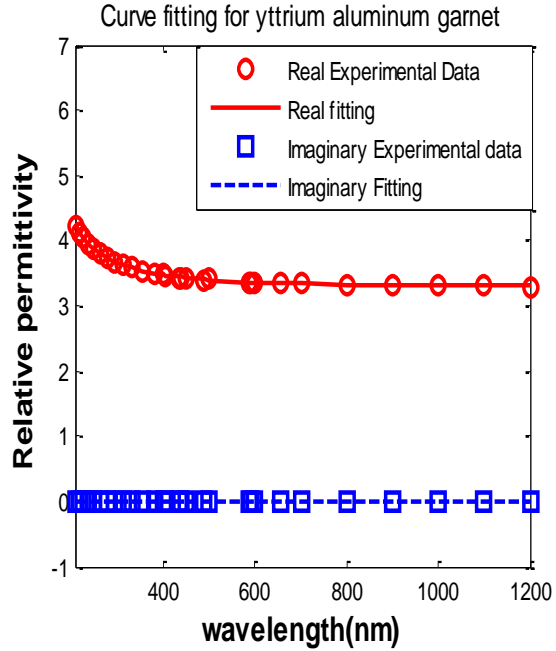


Figure 5.2: Curve fitting for Yttrium Aluminum Garnet

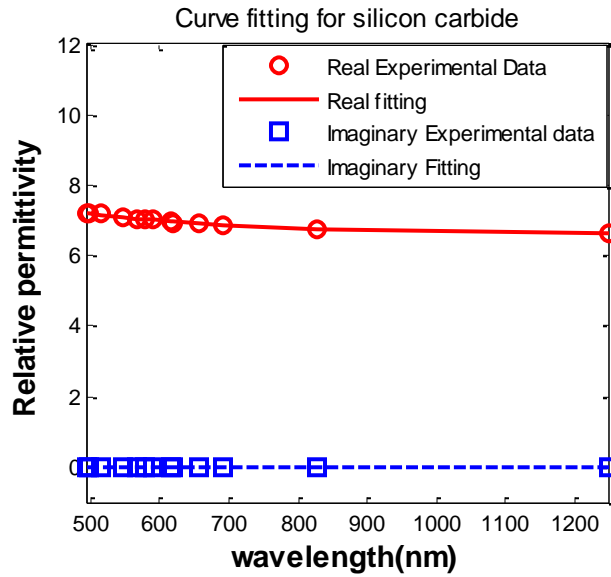


Figure 5.3: Curve fitting for Silicon Carbide

The complex relative permittivity for each material has been determined using both optimized parameters and experimental values. Then the real and imaginary parts have been separated from the complex relative permittivity and plotted which is presented in figures 5.1 to 5.3. The blue colour square and dotted line indicates the

imaginary part of the experimental and fitted data of complex relative permittivity respectively. While the red colour circular and solid line indicates the real part of experimental and fitted complex relative permittivity respectively. From the figure it is clearly visible that the real and imaginary parts of the complex relative permittivity obtained using extracted parameter agrees very well with the real and imaginary parts of the complex relative permittivity obtained from the experimental data [32]. We have used single pole-pair to optimize the Lorentz model parameter for Crystalline Arsenic Sulfide, Yttrium Aluminum Garnet and Silicon Carbide. The more is the number of pole-pairs, the higher the computational time is required. So our single pole-pair model requires significantly less computation time.

5.4.2 Optimized parameter for Dielectric material for modified Lorentz model

Table 5.2: Optimized parameter for Silicon Monoxide for modified Lorentz model

Material	Parameters								
	Wavelength μm	ϵ_{∞}	$\epsilon(\omega)$	No. of pole	$\Delta\epsilon$	ω_p	γ_p	γ_p'	RMS Deviation
SiO	0.30-0.70	1.000010	3.886+0.046i	01	0.843325	0.003269	0.001399	0.007668	0.00873
				02	1.692655	0.053413	0.330511	0.000377	

Two modified Lorentz pole-pair has been used for the extraction of optical parameter for Silicon Monoxide for modified Lorentz model in the wavelength range of 300 nm to 700 nm. From the table 5.2 it seen the RMS deviation is 0.00873 which

indicates the robustness and accuracy of the optimization algorithm. From the Figure 5.4, it is seen that the real and imaginary parts of the complex relative permittivity obtained using extracted parameter agrees very well with the real and imaginary parts of the complex relative permittivity obtained from the experimental data.

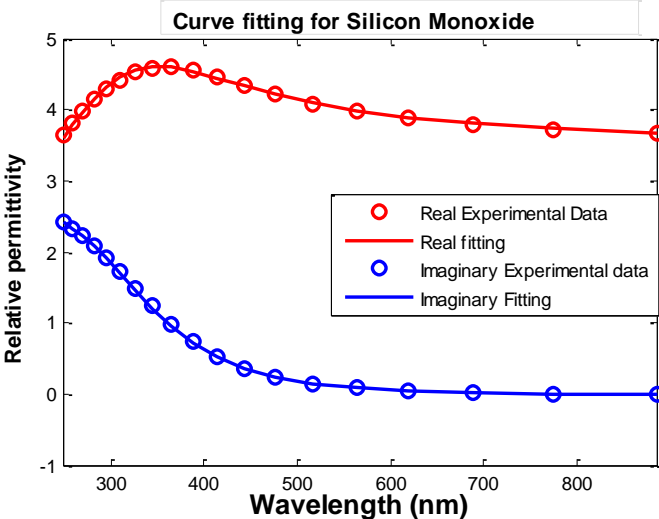


Figure 5.4: Curve fitting for Silicon Monoxide

5.4.3 Optimized parameter for Metal for modified Lorentz model

Table 5.3: Optimized parameter for seven metals for modified Lorentz model

Metals	Parameters								
	Wavelength (μm)	ϵ_{∞}	$\epsilon(\omega)$	No. of pole	$\Delta\epsilon_p$	ω_p	γ_p	γ_p'	RMS deviation
Iridium	0.40-1.378	1.000010	- 42.569 + 47.394i	1	9.812548	0.007721	0.002038	0.365869	0.34571
				2	-6.615408	0.001107	0.018571	24.829479	
				3	3.465769	0.000001	0.010698	24.416921	
				4	10.000000	0.012207	0.270698	25.000000	
Nickel	0.40-1.240	1.000000	- 22.236 + 33.419i	1	9.950488	0.000000	0.130676	24.380180	0.27815
				2	9.817351	0.000714	0.000622	0.018331	
				3	-5.892833	0.038143	0.064130	24.999932	
				4	-1.706868	0.001133	0.006165	8.735793	
				5	9.720442	0.021658	0.216016	14.336483	
Hexagonal Cobalt	0.31-1.088	1.000010	- 22.794 + 30.460i	1	-2.303728	0.000019	0.000046	2.716080	0.06615
				2	7.482513	0.000001	0.000045	0.840162	
				3	-0.130284	0.017380	0.068599	9.498441	
				4	-4.537557	1.439304	1.722500	0.002436	
				5	0.026348	0.004801	0.002629	2.775001	
Palladium	0.30-1.215	1.000009	- 33.894 + 31.796i	1	4.414364	0.003812	0.010677	0.744925	0.05420
				2	-6.444852	0.026238	0.038512	7.995214	
				3	-8.511503	0.000347	0.000118	0.013975	
				4	6.958597	0.000038	0.029772	7.269253	
				5	-1.989911	0.001571	0.005313	5.178818	
				6	9.999941	0.075260	1.463879	0.004552	
Titanium	0.30-.751	1.000010	- 3.992+ 16.341i	1	-7.436450	0.018265	0.297033	8.885233	0.06341
				2	6.453287	0.002265	0.001220	0.004731	
				3	3.237341	0.001320	0.020354	0.777545	
				4	-1.107759	0.271852	0.005674	24.990500	
				5	9.952923	0.052360	0.406145	3.648494	
				6	1.189443	0.023341	0.088210	3.118273	

Table 5.3: Optimized parameter for seven metals for modified Lorentz model (continued)

Metal	Parameters								
	Wavelength h (μm)	ϵ_{∞}	ϵ_s	No. of pole	$\Delta\epsilon_p$	ω_p	γ_p	γ_p'	RMS deviation
Copper	.516-.729	1.00001	- 18.719 + 1.866i	1	0.037490	0.002187	0.000630	2.112530	0.86289
				2	-9.904444	0.032381	0.000000	1.216072	
				3	-10.00000	0.002186	0.000103	0.000000	
				4	-9.965275	0.129588	0.000000	18.784637	
Platinum	.413-1240	1.00000	- 25.330 + 51.953i	1	4.251835	0.025682	0.062638	23.729744	0.08484
				2	7.128254	0.000001	0.002710	0.637786	
				3	-9.999999	0.004847	0.132864	25.000000	
				4	2.880717	0.018043	0.258912	16.869811	

The optimized parameters for the seven metals using large scale non-linear algorithm are presented in table 5.3. From the table it can be observed that a maximum RMS deviation of 0.86289 occurs for Copper which indicates the robustness and accuracy of the optimization algorithm.

The real and imaginary parts have been separated from the complex relative permittivity and plotted which is presented in figures 5.5 to 5.11. The red color indicates the real part while the blue color indicates the imaginary part of the complex relative permittivity. The solid lines denote the extracted parameters and the circle denote the experimental values. From the figure it is clearly visible that

the real and imaginary parts of the complex relative permittivity obtained using extracted parameters agree very well with the real and imaginary parts of the complex relative permittivity obtained from the experimental values [32].

The single pole-pair Debye model parameter obtained by Sagor et al. [33] for Iridium exhibits an RMS deviation of 1.6216 in the wavelength range of 600 nm to 1100nm whereas our obtained four pole-pair modified Lorentz model parameter exhibits an RMS deviation of only 0.34571 in the wavelength range of 400nm to 1378nm. For Nickel, the RMS deviation for the single pole-pair Debye model parameter obtained by Sagor et al.[33] shows an RMS deviation of 1.027 in the wavelength range of 600nm to 1100nm whereas our obtained five pole-pair modified Lorentz parameter shows an RMS deviation of only 0.27815 in the wavelength range of 400 nm to 1240 nm.

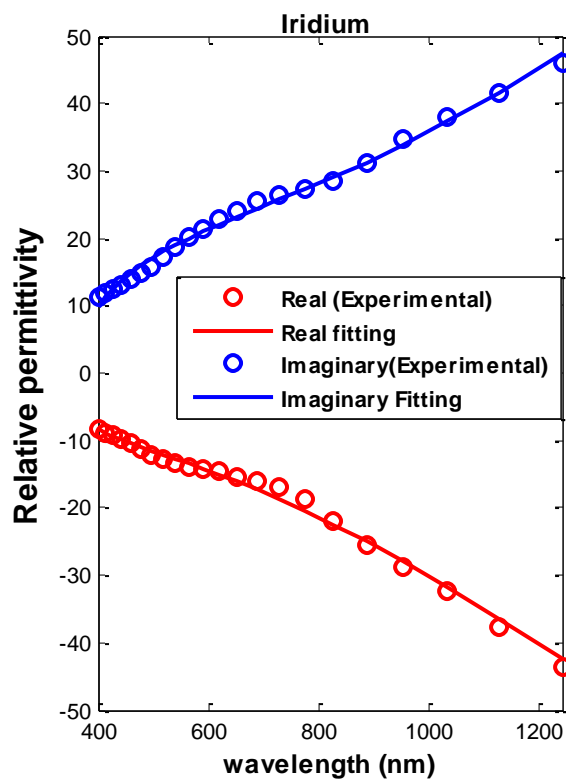


Figure 5.5: Curve fitting for Iridium

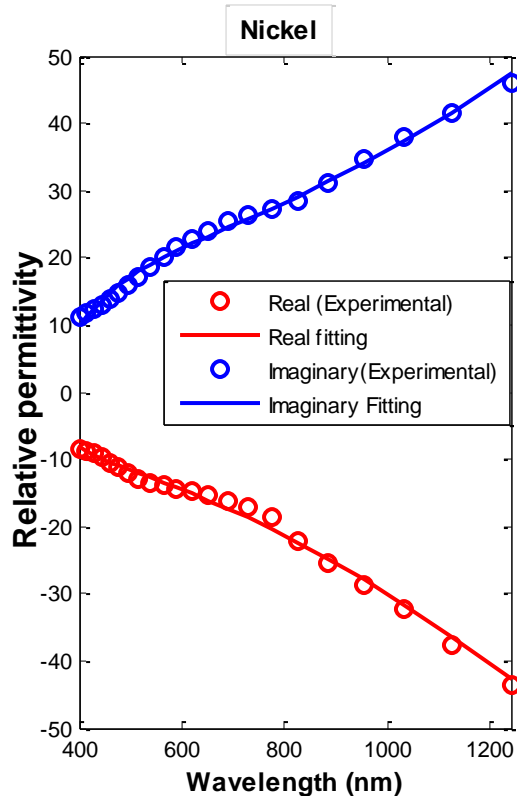


Figure 5.6: Curve fitting for Nickel

For Hexagonal Cobalt, the RMS deviation for the single pole-pair Debye model parameter obtained by Sagor et al.[33] shows an RMS deviation of 1.1510 in the wavelength range of 350nm to 1000nm whereas our obtained five pole-pair modified Lorentz parameter shows an RMS deviation of only 0.06615 in the wavelength range of 310 nm to 1088 nm.

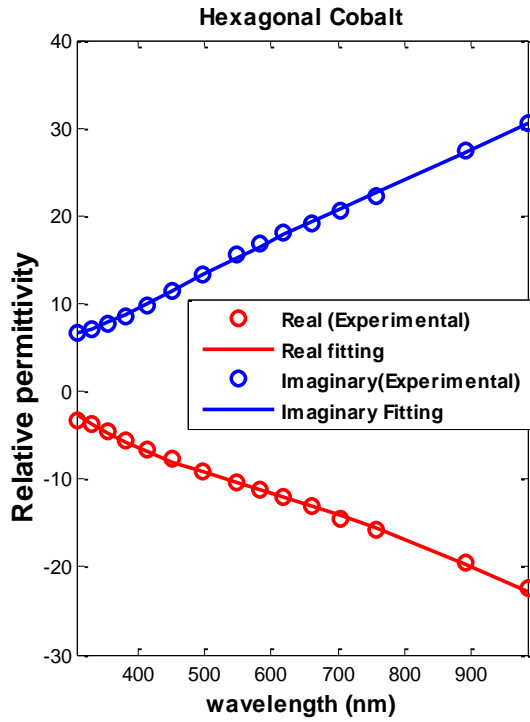


Figure 5.7: Curve fitting for Hexagonal Cobalt

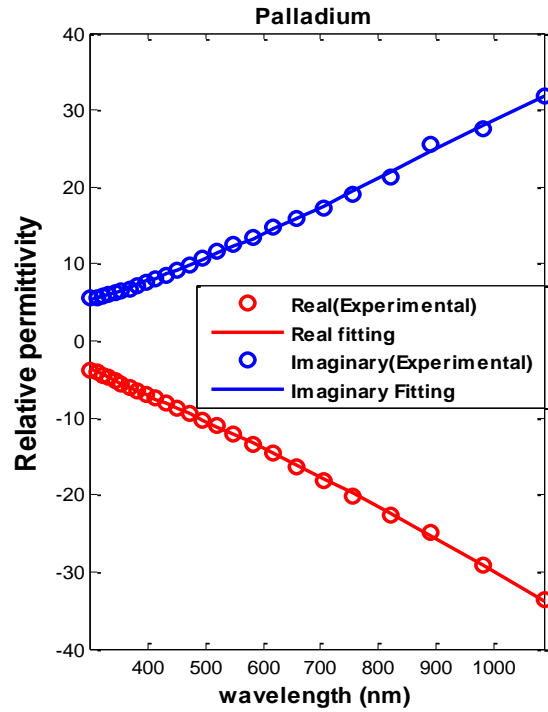


Figure 5.8: Curve fitting for Palladium

For Palladium, the RMS deviation for the single pole-pair Debye model parameter obtained by Sagor et al.[33] shows an RMS deviation of 0.2489 in the wavelength range of 300nm to 700nm whereas our obtained six pole-pair modified Lorentz parameter exhibits an RMS deviation of only 0.05420 in the wavelength range of 300 nm to 1215nm.

The single pole-pair Debye model parameter obtained by Sagor et al. [33] for Titanium exhibits an RMS deviation of 1.1239 in the wavelength range of 400nm to 700nm whereas our obtained six pole-pair modified Lorentz model parameter exhibits an RMS deviation of only 0.06341 in the wavelength range of 300nm to 751nm.

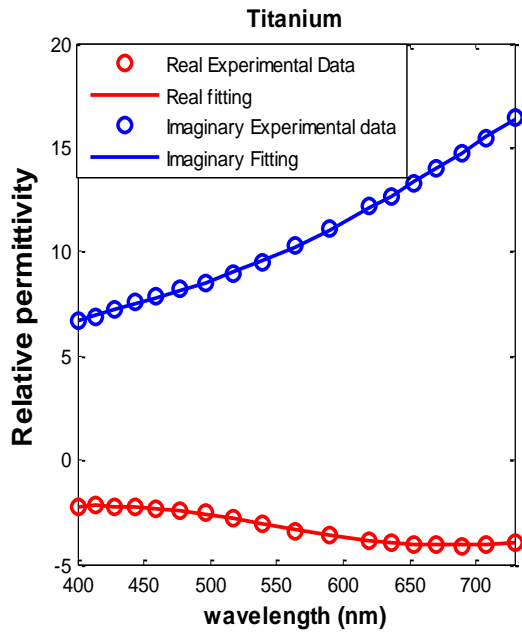


Figure 5.9: Curve fitting for Titanium

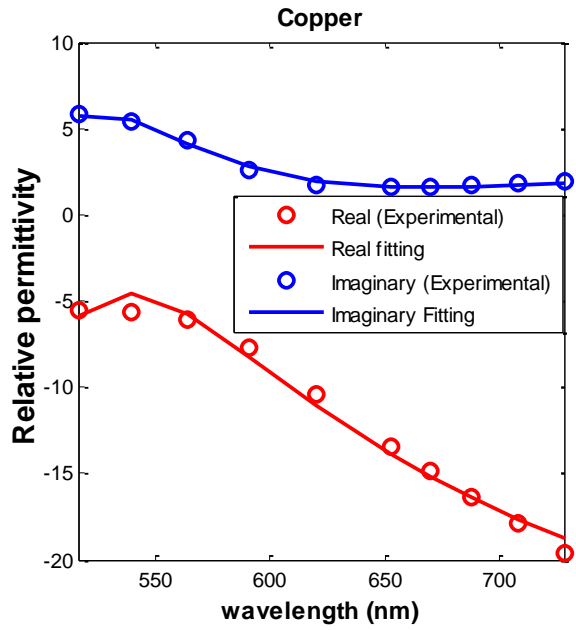


Figure 5.10: Curve fitting for Copper

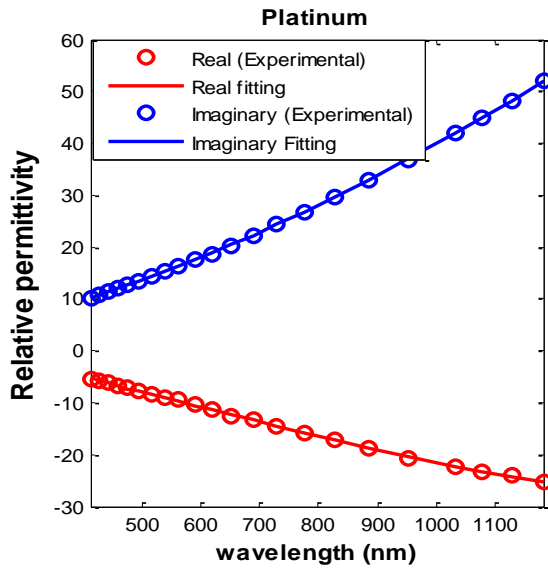


Figure 5.11: Curve fitting for Platinum

Similarly from the table it is seen that the RMS deviation for Copper and Platinum is also minimum i.e. 0.86289 and 0.08484 respectively. In case of Copper and Platinum, we have used four pole-pair and five pole-pair for the extraction of modified Lorentz parameter.

In general, all models of metals have a negative real part of permittivity in most of the frequency range. The imaginary part, which is responsible for attenuation, is very large in most of the frequency range. The very large imaginary part causes EM waves to attenuate very fast inside the metal. That is why metals are considered as perfect conductors. In the optical range, metals have a reasonably small imaginary part and a reasonably small negative real part, as shown in above figure. Because of this, SPPs have the ability to propagate in metals.

Chapter 6

Application and Case Study

6.1 Simulation model

An FDTD method [22] based model has been used for simulation purpose. Here, the general auxiliary differential equation (ADE) based FDTD [34] approach has been utilized to incorporate the frequency dependent dispersion property of the constituent material. This algorithm is useful for the simulation of materials with different dispersive properties. The perfectly matched layer [35] has been integrated at all the boundaries in order to prevent back reflections.

Considering the dispersion property of material the frequency-dependent electric flux density can be expressed as

$$D(\omega) = \varepsilon_o \varepsilon_\infty E(\omega) + P(\omega) \quad (6.1)$$

The general Lorentz model is given by

$$P(\omega) = \frac{a}{b + jc\omega - d\omega^2} E(\omega) \quad (6.2)$$

Using inverse Fourier transform, above equation can be written as

$$bP(t) + cP'(t) + dP''(t) = aE(t) \quad (6.3)$$

The FDTD solution for the first order polarization of Eq. (6.3) can be given as

$$P^{n+1} = C_1 P^n + C_2 P^{n-1} + C_3 E^n \quad (6.4)$$

$$\text{Where, } C_1 = \frac{4d - 2b\Delta t^2}{2d + c\Delta t}, C_2 = \frac{-2d - c\Delta t}{2d + c\Delta t} \text{ and } C_3 = \frac{2a\Delta t^2}{2d + c\Delta t}$$

The values of C_1 , C_2 and C_3 depend on the material under consideration. Finally the electric field intensity becomes

$$E^{n+1} = \frac{D^{n+1} - \sum_{i=1}^N P_i^{n+1}}{\epsilon_o \epsilon_\infty} \quad (6.5)$$

Where N is the number of pole-pair and D^{n+1} is the update value of the electric flux density calculated by using FDTD algorithm.

6.2 Numerical Results for Temporal Solitons

In this section the dynamics of temporal solitons calculated using ADE non-linear dispersion algorithm for the FDTD method has been presented. Single pole-pair Lorentz model parameters of As_2S_3 is used to demonstrate the dispersion of a secant wave while propagating through As_2S_3 . The pulse that we have used is of unity amplitude of its electric field with a carrier frequency of 1.37×10^{14} Hz. The grid resolution was set at 5nm. The below figure depicts the result of dispersive ADE-FDTD computation. In Fig. 6.1, the computed rightward propagating pulse for the Lorentz dispersive case is plotted at 20000 and 40000 time-steps. The parameters used for simulation is as follows:

$$\epsilon_\infty = 1.000010, \epsilon_s = 8.291, \omega_o = 6.7425 \times 10^{15} (\text{rad / sec}) \text{ and } \delta = 1.885 \times 10^{11} (\text{rad / sec}).$$

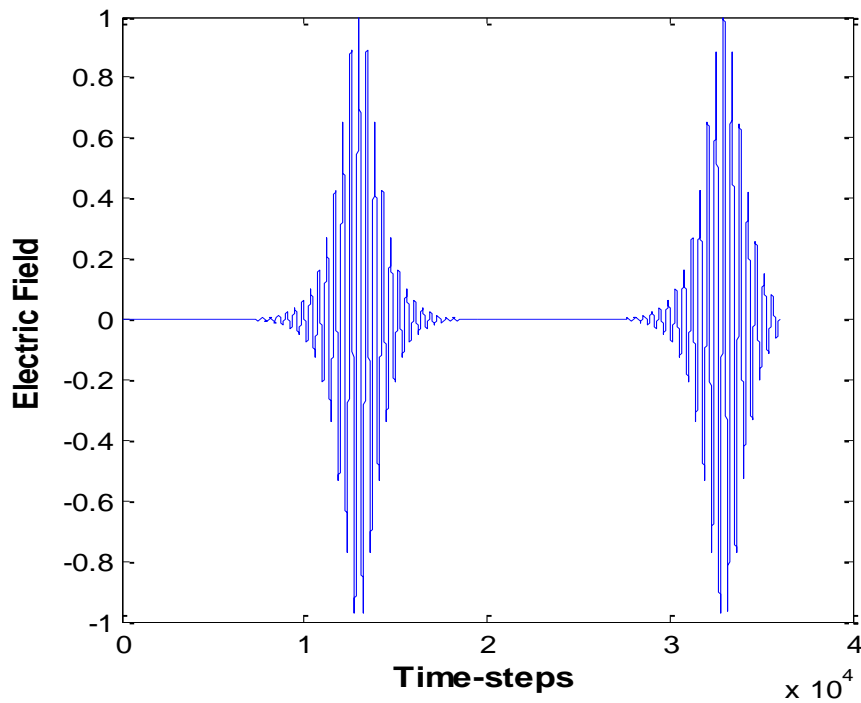


Figure 6.1 Calculated optical pulse after 20,000 and 40,000 time-steps

6.3 Plasmonic Waveguide

In this section, the FDTD simulator is used to study plasmonic waveguides. SPPs are electromagnetic waves propagating on the surface between two media: dielectric and metal. Here, we have investigated the symmetric SPP propagation properties in dielectric-metal-dielectric waveguide where As_2S_3 is used as dielectric material and Ag as metal. The schematic view of metal-dielectric-metal waveguide that we have used for simulation is given in figure 6.2. The width of the metal layer has been taken as 300 nm and width of both dielectric layers as 850 nm. Here, input plane type light source has been used which can propagate in a particular direction and has an

intensity distribution across the incident plane. The profile pumped into DMD waveguide is given in figure 6.3 and in figure 6.4.

The SPP wavelength is given by,

$$\lambda_{SPP} = \lambda_o \sqrt{\frac{\epsilon_d + \epsilon_m'}{\epsilon_d \epsilon_m'}} \quad (6.6)$$

Where, λ_o is the free space wavelength, ϵ_d is the real part of the complex relative permittivity of dielectric and ϵ_m' is the real part of the complex relative permittivity of the metal.

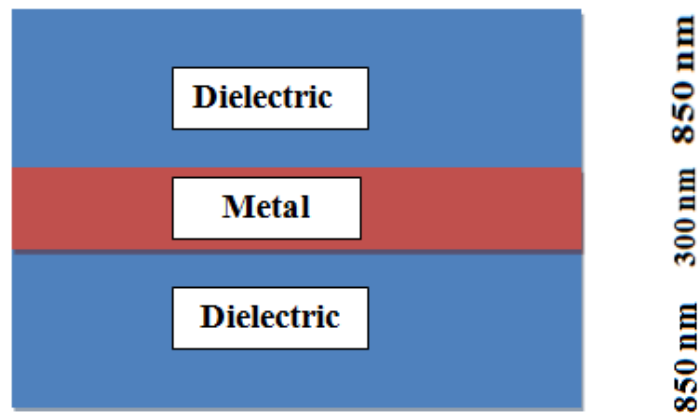


Figure 6.2: Schematic diagram of the DMD waveguide used for simulation.

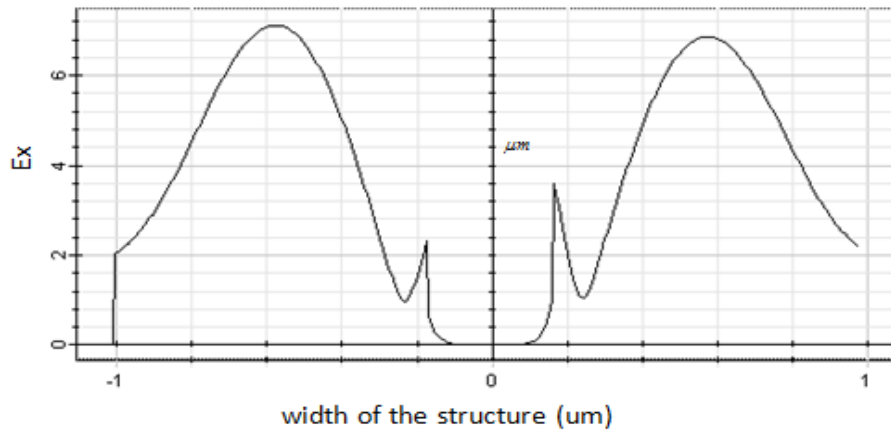


Figure 6.3: E_x profile pumped into DMD waveguide

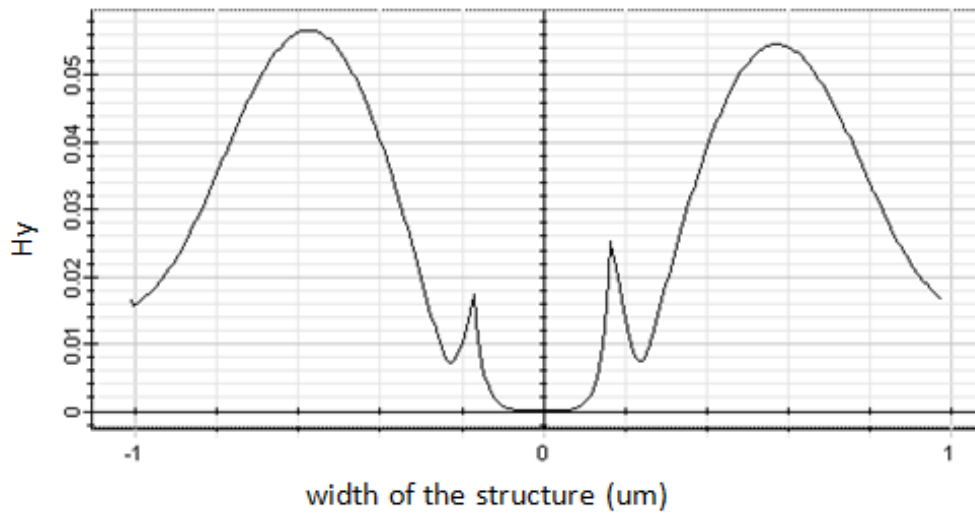


Figure 6.4: H_y profile pumped into DMD waveguide

In figure 6.5 to figure 6.10 the field distributions are shown in both time domain and frequency domain.

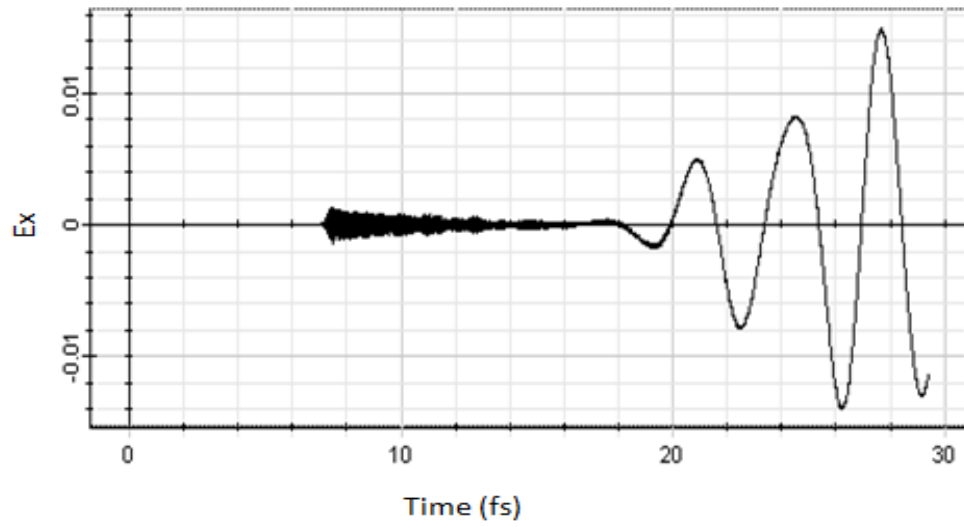


Figure 6.5: E_x profile at different time instant

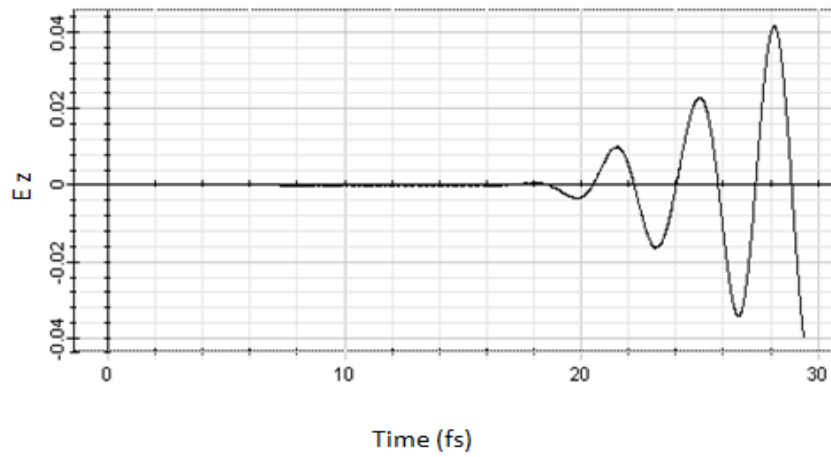


Figure 6.6: E_z profile at different time instant

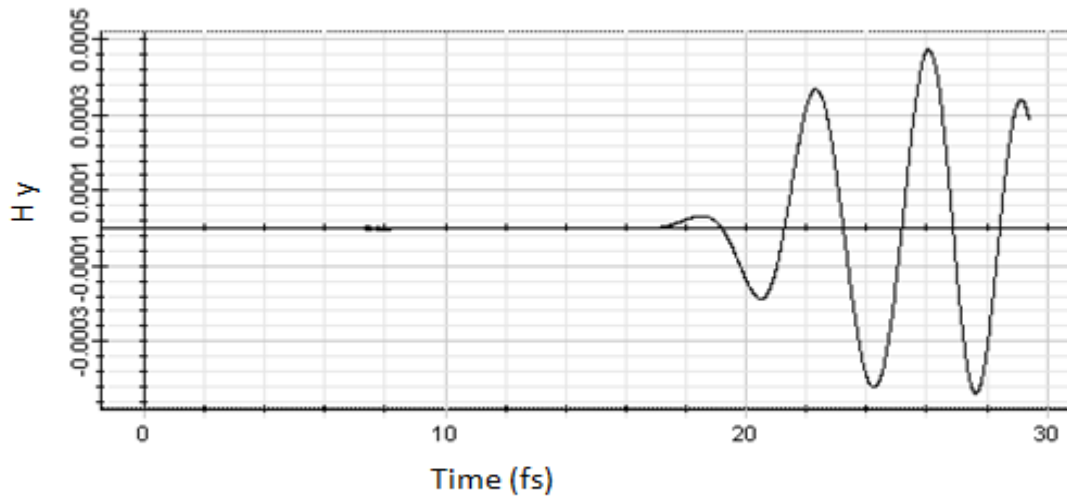


Figure 6.7: H_y profile at different time instant

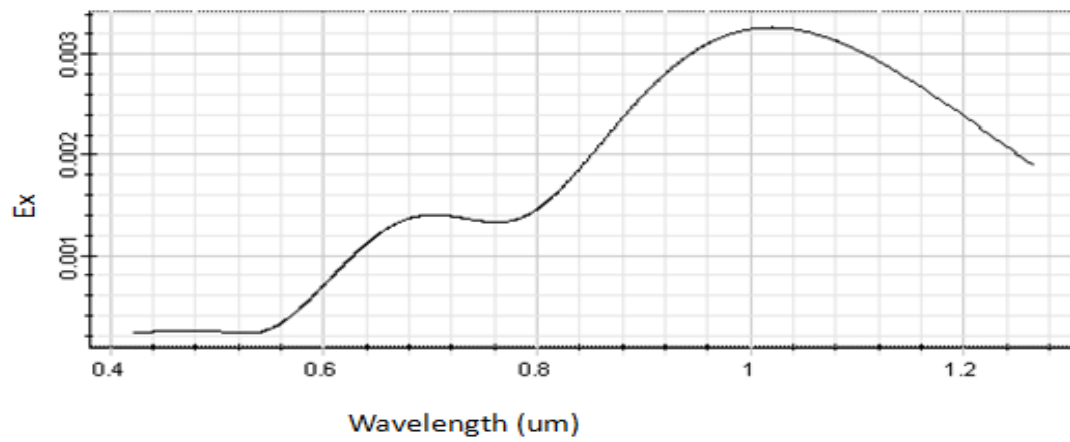


Figure 6.8: E_x field strength at different distance

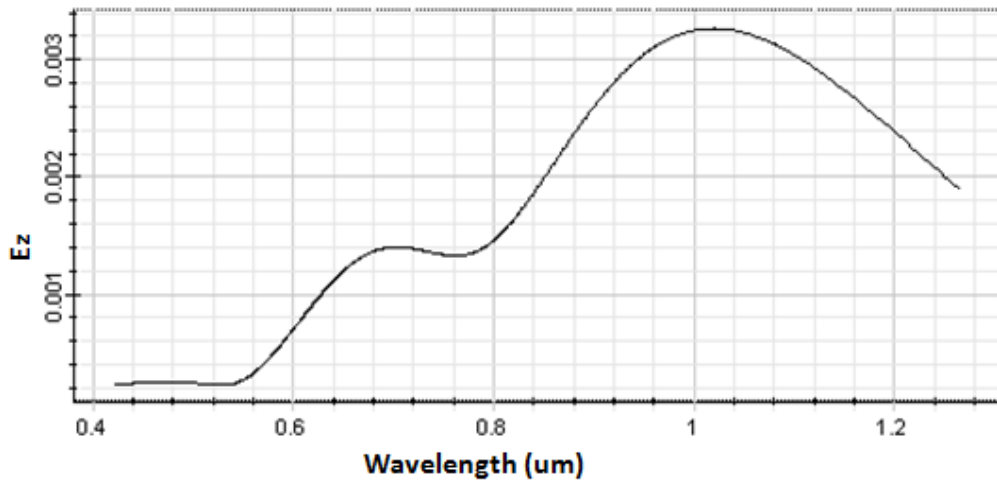


Figure 6.9: E_z field strength at different distance

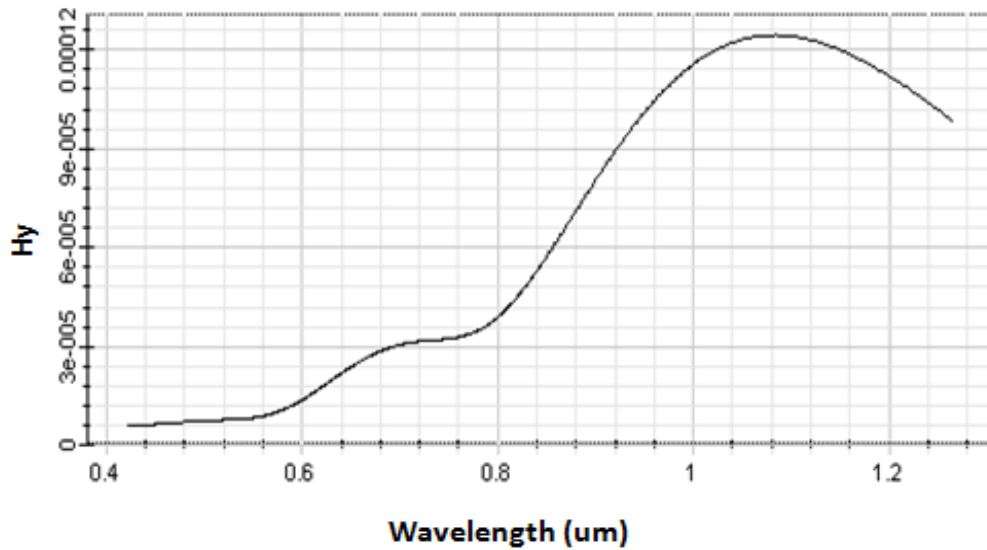


Figure 6.10: H_y field strength at different distance

The variation in electric field strength (2D) in different time steps at different distances from the dielectric metal interface are presented in figure 6.11

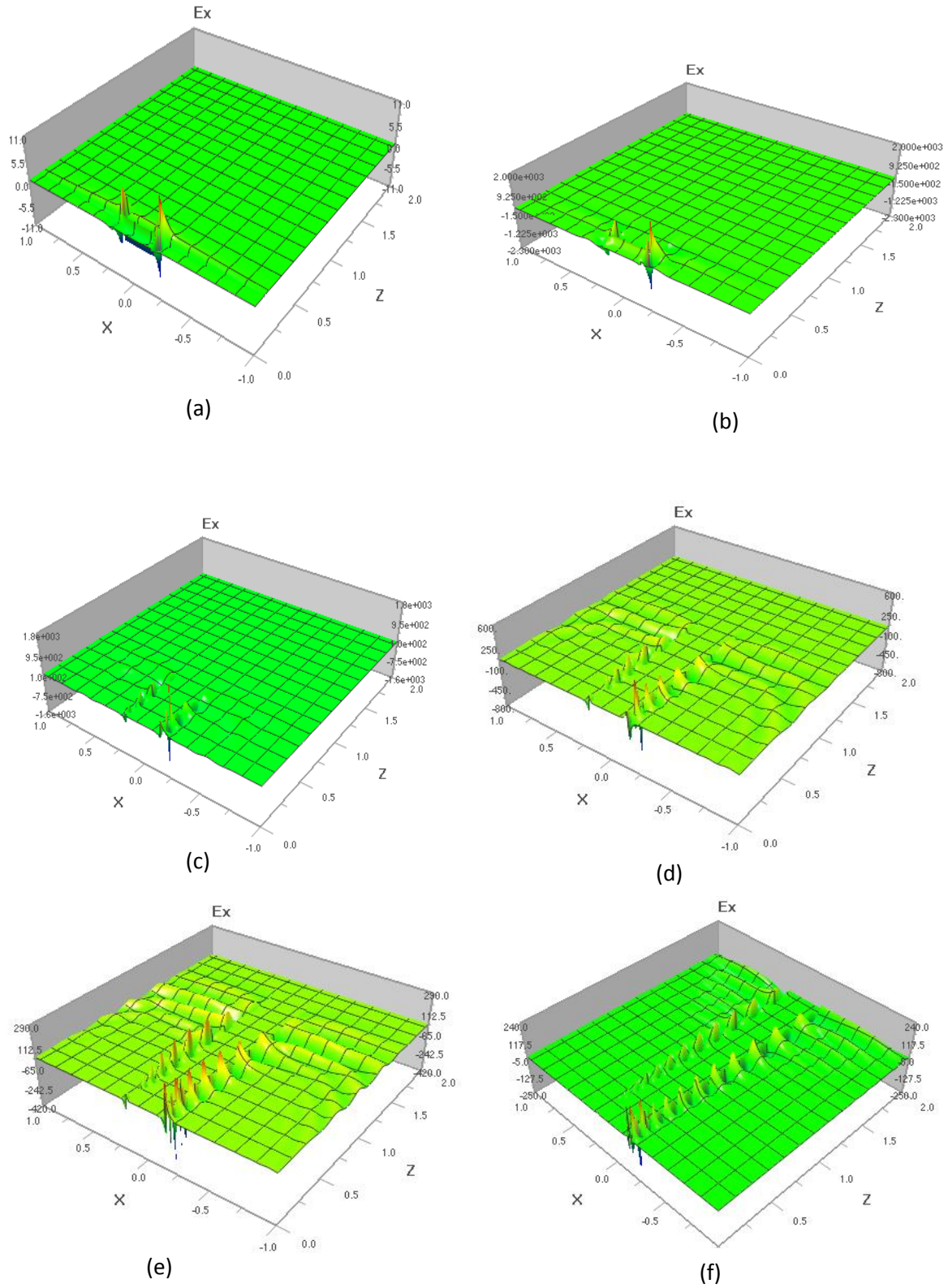


Figure 6.11: 2D Electric field distribution inside the DMD waveguide used for simulation at time step (a) 100 (b) 500 (c) 950 (d) 1400 (e) 1750 (f) 2646

It can be observed that the electric field strength decreases as one goes away from the interface. This is the reason SPP mode field decreases exponentially in strength as one goes further from the interface in the y-direction. Due to the skin effect of the SPP mode in the metal and dielectric layers it happens. The resonance mode is also clearly visible in the figures with peak amplitudes centered on different input signal wavelength for different materials. Figure 6.12 depicts the power transmission efficiency of the DMD waveguide. The efficiency is determined by measuring input source power at the starting point of the metal channel and received power at the end of the metal channel.

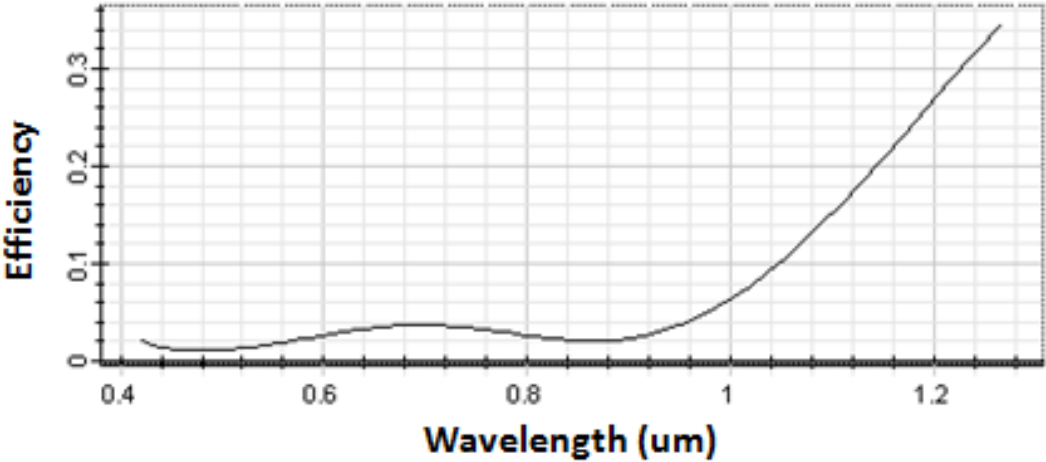


Figure 6.12: Power transmission efficiency at different distances.

Chapter 7

Conclusion and Future Works

7.1 Summary and Conclusion

The main contribution of this thesis is the extraction of modeling parameters for several materials and the analysis of a coupling structure using Silver as metal and Arsenic Sulfide as dielectric. In this thesis, investigations of the propagation of SPPs in the nanostructure were done and field distribution inside the waveguide has been analyzed. In near future, SPPs can take the role of electrons to reach better and smaller devices. The thesis can be summarized as follows:

- ❖ A large scale nonlinear optimization method has been described and the modeling parameters for several metals and dielectric materials have been extracted in the visible and near-IR range of the electromagnetic spectrum. The comparison between the optimized result and experimental result has been shown to prove the validity of the optimization method.
- ❖ An ADE-FDTD algorithm based two dimensional simulation model has been developed in order to simulate optical nanostructures. The validity of the simulation model has been checked by simulating with the parameters given by Taflove and comparing the results provided by Taflove [11]. Then the dynamics of temporal solitons has been calculated for Arsenic Sulfide using the simulation model. In this case single pole-pair Lorentz model parameter of Arsenic Sulfide has been used.

- ❖ Electric field distribution in dielectric-metal-dielectric waveguide has been analyzed for Arsenic Sulfide (dielectric) and Silver (metal) and power transmission efficiency at different distances has been shown.

7.2 Future Works

Work in this very interesting field can be extended in many directions.

- ❖ We will investigate metal-dielectric-metal waveguide with a combiner constructed with different dielectric materials.
- ❖ We will investigate metal-dielectric-metal waveguide with a combiner constructed with different dielectric materials.
- ❖ We will investigate SPP propagation characteristics in different DMD waveguide. The characteristics that will be focused are SPP wavelength, SPP penetration depth and electric field strength at different distances from the metal-dielectric surface.
- ❖ The current numerical simulator can be extended to 3D to observe the linear dispersion of different nanostructures.
- ❖ We will try to arrange some experimental setups and implement our work practically.

Bibliography

- [1] S. Y. Chou and W. Ding, "Ultrathin, high-efficiency, broad-band, omni-acceptance, organic solar cells enhanced by plasmonic cavity with subwavelength hole array," *Optics express*, vol. 21, pp. A60-A76, 2013.
- [2] S.-S. Kim, *et al.*, "Plasmon enhanced performance of organic solar cells using electrodeposited Ag nanoparticles," *Applied Physics Letters*, vol. 93, p. 073307, 2008.
- [3] S. Pillai, *et al.*, "Surface plasmon enhanced silicon solar cells," *Journal of applied physics*, vol. 101, p. 093105, 2007.
- [4] R. J. Blaikie and D. O. Melville, "Imaging through planar silver lenses in the optical near field," *Journal of Optics A: Pure and Applied Optics*, vol. 7, p. S176, 2005.
- [5] D. Melville and R. Blaikie, "Super-resolution imaging through a planar silver layer," *Optics express*, vol. 13, pp. 2127-2134, 2005.
- [6] S. Kawata, *et al.*, "Plasmonics for near-field nano-imaging and superlensing," *Nature Photonics*, vol. 3, pp. 388-394, 2009.
- [7] X. Zhang and Z. Liu, "Superlenses to overcome the diffraction limit," *Nature materials*, vol. 7, pp. 435-441, 2008.
- [8] A. J. Haes and R. P. Van Duyne, "A unified view of propagating and localized surface plasmon resonance biosensors," *Analytical and Bioanalytical Chemistry*, vol. 379, pp. 920-930, 2004.
- [9] A. Hosseini and Y. Massoud, "A low-loss metal-insulator-metal plasmonic bragg reflector," *Optics express*, vol. 14, pp. 11318-11323, 2006.
- [10] J. Henzie, *et al.*, "Multiscale patterning of plasmonic metamaterials," *Nature nanotechnology*, vol. 2, pp. 549-554, 2007.
- [11] A. Taflove and S. C. Hagness, "Computational Electrodynamics," 2000.
- [12] T. Onuki, *et al.*, "Propagation of surface plasmon polariton in nanometre-sized metal-clad optical waveguides," *Journal of microscopy*, vol. 210, pp. 284-287, 2003.
- [13] M. L. Brongersma and P. G. Kik, *Surface plasmon nanophotonics*: Springer, 2007.
- [14] M. Hochberg, *et al.*, "Integrated plasmon and dielectric waveguides," *Optics express*, vol. 12, pp. 5481-5486, 2004.
- [15] Y. Liu, *et al.*, "Finite-difference time-domain simulation of plasmonic nanoparticles," in *Antennas and Propagation Society International Symposium 2006, IEEE*, 2006, pp. 741-744.
- [16] J. T. Krug II, *et al.*, "Design of near-field optical probes with optimal field enhancement by finite difference time domain electromagnetic simulation," *The Journal of chemical physics*, vol. 116, pp. 10895-10901, 2002.
- [17] W. H. Pernice, *et al.*, "A general framework for the finite-difference time-domain simulation of real metals," *Antennas and Propagation, IEEE Transactions on*, vol. 55, pp. 916-923, 2007.
- [18] A. D. Rakic, *et al.*, "Optical properties of metallic films for vertical-cavity optoelectronic devices," *Applied optics*, vol. 37, pp. 5271-5283, 1998.
- [19] C. A. Balanis, *Advanced engineering electromagnetics* vol. 20: Wiley New York, 1989.
- [20] F. L. Pedrotti, *et al.*, *Introduction to optics* vol. 2: Prentice-Hall Englewood Cliffs, 1993.
- [21] A. Deinega and S. John, "Effective optical response of silicon to sunlight in the finite-difference time-domain method," *Optics letters*, vol. 37, pp. 112-114, 2012.
- [22] K. S. Yee, "Numerical solution of initial boundary value problems involving Maxwell's equations," *IEEE Trans. Antennas Propag*, vol. 14, pp. 302-307, 1966.
- [23] J. N. Reddy, *An introduction to the finite element method* vol. 2: McGraw-Hill New York, 1993.
- [24] D. M. Sullivan, "Frequency-dependent FDTD methods using Z transforms," *Antennas and Propagation, IEEE Transactions on*, vol. 40, pp. 1223-1230, 1992.
- [25] D. M. Sullivan, "Z-transform theory and the FDTD method," *Antennas and Propagation, IEEE Transactions on*, vol. 44, pp. 28-34, 1996.

- [26] R. Luebbers, *et al.*, "A frequency-dependent finite-difference time-domain formulation for dispersive materials," *Electromagnetic Compatibility, IEEE Transactions on*, vol. 32, pp. 222-227, 1990.
- [27] D. F. Kelley and R. J. Luebbers, "Piecewise linear recursive convolution for dispersive media using FDTD," *Antennas and Propagation, IEEE Transactions on*, vol. 44, pp. 792-797, 1996.
- [28] J. L. Young, *et al.*, "On the dispersion errors related to (FD) 2 TD type schemes," *Microwave Theory and Techniques, IEEE Transactions on*, vol. 43, pp. 1902-1910, 1995.
- [29] X. Ai, *et al.*, "Analysis of dispersion relation of piecewise linear recursive convolution FDTD method for space-varying plasma," *Progress In Electromagnetics Research Letters*, vol. 22, pp. 83-93, 2011.
- [30] T. Körner and W. Fichtner, "Dispersive media in fdtd-comparison of recursive convolution and auxiliary differential equation methods," in *Technical Proceedings of the 1998 International Conference on Modeling and Simulation of Microsystems*, 1998, pp. 339-343.
- [31] I. Valuev, *et al.*, "Implementation of the iterative finite-difference time-domain technique for simulation of periodic structures at oblique incidence," *Computer Physics Communications*, 2014.
- [32] E. D. Palik, *Handbook of optical constants of solids* vol. 3: Academic press, 1998.
- [33] R. H. Sagor, *et al.*, "An optimization method for parameter extraction of metals using modified Debye model," *SpringerPlus*, vol. 2, p. 426, 2013.
- [34] M. A. Alsunaidi and A. A. Al-Jabr, "A general ADE-FDTD algorithm for the simulation of dispersive structures," *Photonics Technology Letters, IEEE*, vol. 21, pp. 817-819, 2009.
- [35] J.-P. Berenger, "A perfectly matched layer for the absorption of electromagnetic waves," *Journal of computational physics*, vol. 114, pp. 185-200, 1994.